UNITED NATIONS UNIVERSITY
GEOTHERMAL TRAINING PROGRAMME
Orkustofnun, Grensasvegur 9,
IS-108 Reykjavik, Iceland

Report 2012
Number 35

1D JOINT INVERSION OF TEM AND MT RESISTIVITY DATA WITH AN APPLICATION OF SOUNDINGS FROM THE NÁMAFJALL HIGH-TEMPERATURE GEOTHERMAL AREA, NE-ICELAND

Mohammad Zohir Uddin
Geological Survey of Bangladesh
153, Pioneer Road, Segunbagicha
Dhaka 1000
BANGLADESH
zohir.uddin@gmail.com

ABSTRACT

Geophysical methods are most useful in extracting subsurface information. Which geophysical method should be used to characterize a site depends on what information one needs. Resistivity has a direct relationship with the subsurface rock temperature. TEM and MT are very cost effective methods in a subsurface resistivity study. Although the MT method is very efficient at getting information down to the mantle, it suffers a static shift problem. Joint interpretation of TEM and MT data removes the static shift from MT data. Geologically, Námafjall is a very important area in Iceland. Tectonically it is related to Krafla volcano. It was formed in subglacial eruptions during the last glaciation and has undergone cooling. In this study sixteen TEM and MT soundings were used to evaluate the subsurface resistivity. At shallow depth there is a low-resistivity layer having resistivity less than 10 Ωm below Námafjall ridge. On the surface this area coincides with surface geothermal manifestations. It signifies the presence of low-temperature alteration minerals, mainly zeolites and smectite. Resistivity values above this low-resistivity cap indicate the presence of unaltered fresh rock. Below 200 m b.s.l., high resistivity values below the low resistivity signify high-temperature alteration minerals, mostly chlorite and epidote. At about 800 m depth, there is again a low-resistivity layer at the northernmost site, indicative of a fracture zone which might be connected to the Krafla volcano. A low-resistivity zone with resistivity of less than 5 Ωm is also found from 2 km to 10 km b.s.l. This low-resistivity zone signifies a probable heat source for Námafjall area. Electrical strike analysis and Tipper study suggest a conductive zone at less than 1 km depth and the presence of fractures at different depths that are not always parallel to the major geological structures.

1. INTRODUCTION

Iceland is an advanced country in the use of geothermal energy. The country started using geothermal energy in the 1930s. Close to 30% of the electricity is now produced by geothermal resources and 90% of the houses in Iceland are heated up by geothermal energy. For optimal use of geothermal power, geoscientists in Iceland developed different technological disciplines. Geophysical exploration is one of the technological disciplines that are used very effectively in exploration, development and

sustainable use of geothermal energy. Resistivity, seismic, gravity and magnetic methods are used separately or combined at different stages in geothermal exploration, development and exploitation. Of all the above mentioned geophysical methods, only resistivity has a direct relationship with subsurface temperature. Before 1980, when the TEM and MT methods were not fully developed, geoscientists generally used vertical electrical soundings (VES) in the exploration stage for site characterization and also for the selection of suitable drilling targets.

FIGURE 1: Position of Bangladesh and Thakurgaon District (modified from Wikipedia, 2012)

2. PURPOSE OF THE STUDY

Bangladesh is a developing nation in South Asia and is situated on the eastern side of India. The country needs energy for its development. Recently, geoscientists in Bangladesh found a prospective area for exploitation of geothermal energy in the northernmost district of Bangladesh (Thakurgaon) (Rahman, 2006; Guha and Henkel, 2005; Guha et al., 2010) (Figure 1). Since the country only recently discovered a prospective area for geothermal power, it has no prior knowledge on how to explore the energy resource. Knowledge of geophysical exploration would help in exploring and developing this recently discovered geothermal field. Bangladesh is a densely populated country where more than 900 people live per square kilometre; therefore, it could be quite difficult to find a 2 km long straight line for VES soundings. Knowledge of MT and TEM soundings could help to improve the depth of penetration by using the small amounts of available suitable open areas in the country.

3. RESISTIVITY OF ROCK

3.1 Specific resistivity

Electrical resistivity of a material, ρ (ohm-m or Ωm) is directly proportional to the voltage difference ΔV, between two ends of a material, having length L and cross-sectional area A and indirectly proportional to the current I, that passes through it:

$$\rho = R\frac{A}{L} = \frac{\Delta V A}{I\,L} \tag{1}$$

where ρ = Specific resistivity of the material (Ωm);
R = Electrical resistance of the material (Ω);
A = Cross-sectional area of the conducting material (m^2);
L = Length (m).

The reciprocal value of resistivity is conductivity σ, and its unit is Siemens/m. Materials which have high resistivity generate high heat during electron conductions (Hersir and Árnason, 2009).

3.2 Factors affecting the resistivity of rocks

The resistivity of geological materials depends on various factors. These are grain to grain contact, fluid contents, dissolved solids in the fluid, compaction of the rock, secondary porosity, temperature, texture of the grains and alteration of minerals due to high pressure and temperature.

3.2.1 Lithology

Resistivity of rocks is dependent on mineralogical compositions (Figure 2). Rocks which are composed of nonconductive minerals (Quartz, Calcite, and Gypsum) show high resistivity compared to rock units that are composed of conductive minerals (Kearey et al., 2002). The mineralogical composition of a rock unit in a high-temperature area depends on the source material of the magma and subsequent alteration due to the interaction of minerals and pore fluid at high-temperature. The resistivity distribution in high-temperature areas in Iceland does not only depend on mineralogical composition but also on the alteration of minerals.

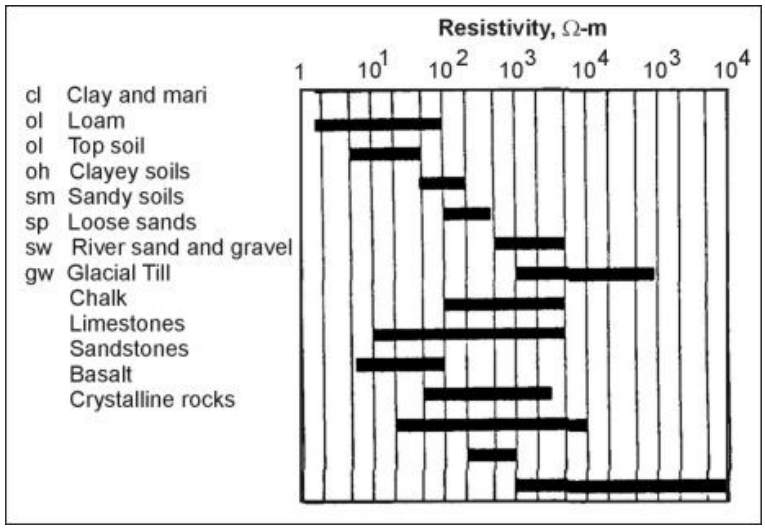

FIGURE 2: Resistivity of different rock types (USDOT, 2012)

3.2.2 Porosity and permeability

The porosity of a rock unit is defined as the ratio of the pore space in rock which is not occupied by minerals to the total volume of the rock (Equation 2). There are three types of porosity. These are inter granular (pores formed as spaces between the grains), joint-fissures and vugular (big and irregular pores formed as a material is dissolved or washed away). Equation 2 defines porosity:

$$\emptyset_t = \frac{V_\varphi}{V} \tag{2}$$

where V_φ = Volume of space not occupied by minerals (m^3);
$\emptyset_t$ = Fractional porosity;
V = Total volume of the rock (m^3).

Resistivity depends on the pore fluid as described by Archie's law (Hersir and Árnason, 2009):

$$\rho = \rho_w a \emptyset_t^{-n} \tag{3}$$

where ρ = Bulk resistivity (Ωm);
ρ_w = Resistivity of the pore fluid (Ωm);
a = An empirical parameter, usually around 1;
n = Cementing factor which varies from 1 to 2, depending on the rock type.

Permeability represents fluid flow through a porous media. A rock may be highly porous, but if the pores are not interconnected then the rock is not permeable. If the pores are interconnected, then it is called effective porosity. Usually permeability is directional and follows a certain direction of the rock unit. Secondary porosity such as a fracture has a significant effect on the total permeability of the rock

unit of igneous origin. In volcanic areas, secondary permeability determines the major zone of fluid flow.

In addition to the characteristics of the host materials, the viscosity and pressure of the fluid also determine the rate at which the fluid will flow. The fluid flow also controls resistivity. Permeability k is measured in milliDarcy - mD (Heath, 2004):

$$k = \frac{QL\mu}{A(P_a - P_b)} \tag{4}$$

where Q = Total discharge (m^3/s);
A = Cross-sectional area (m^2);
$P_a - P_b$ = Pressure drop over length L (Pa);
L = Length along which pressure drops (m);
μ = Viscosity (Pa-s);
k = Permeability (D).

With increasing dissolved solids, resistivity decreases.

3.2.3 Temperature

Resistivity generally increases with increasing temperature in metals. But in aqueous solutions, the resistivity generally decreases up to 200°C temperature, then it starts to increase again (Figure 3). Dakhnov (1962) described the relationship between temperature and the resistivity of rocks saturated with an electrolyte (Equation 5).

$$\rho_w = \frac{\rho_{w_o}}{1 + \alpha(T - T_0)} \tag{5}$$

where ρ_w = Resistivity of the fluid at temperature T (Ωm);
α = Temperature coefficient of resistivity (°C $^{-1}$);
T_0 = Reference temperature (°C);
ρ_{w_o} = Resistivity of the fluid at temperature T_0 (Ωm).

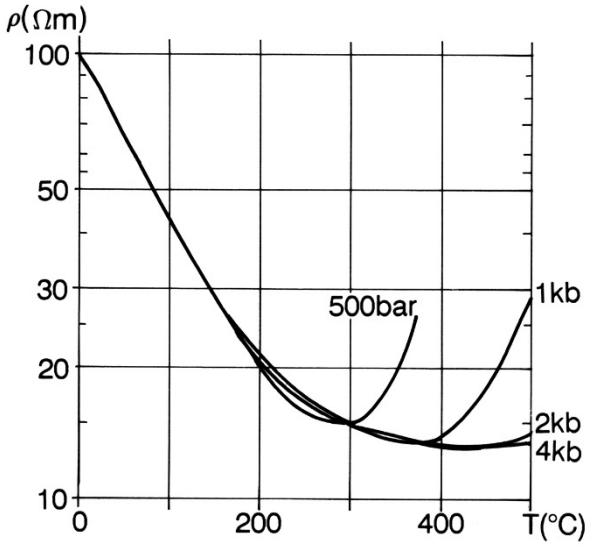

FIGURE 3: Resistivity versus temperature of a NaCl solution (Hersir and Björnsson, 1991; modified from Quist and Marshall, 1968)

Generally the dielectric permittivity of the water decreases at higher temperature which lowers the dissociation power of the solution. At temperature higher than 300°C, this phenomenon increases the resistivity (Quist and Marshall, 1968).

3.2.4 Resistivity and alteration of rocks

In high-temperature areas in volcanic regions like in Iceland, the subsurface materials can be divided into three sections on the basis of resistivity, alteration and temperature (Figure 4). The top-layer has a temperature of less than 50-100°C and high resistivity compared to the rest of the layers. The surface layer is usually not altered and the conduction generally occurs through the pore fluid. The second layer has a temperature of 100-230°C and low resistivity compared both with the upper layer or the bottom layer (Pytte and Reynolds, 1989; Tucker, 1991). Due to moderate temperature and pressure, this layer is somewhat altered and the alteration minerals are mainly

smectite-zeolites and mixed-layer clays. The presence of clay minerals in the second layer make it different from the top layer and the electron flow through this zone mainly occurs by surface conduction (Figure 5). Generally, smectite type clay has a negatively charged free surface with loosely bound positive charges and these charges are responsible for surface conduction (Figure 6). This phenomenon lowers the resistivity of the second layer. The third layer has a higher resistivity than the second layer. It has a temperature higher than 230°C. The alteration mineral composition of this zone is mainly chlorite and epidote. Chlorite and epidote have no loosely bound cations. The conduction here is therefore both surface and pore fluid conduction.

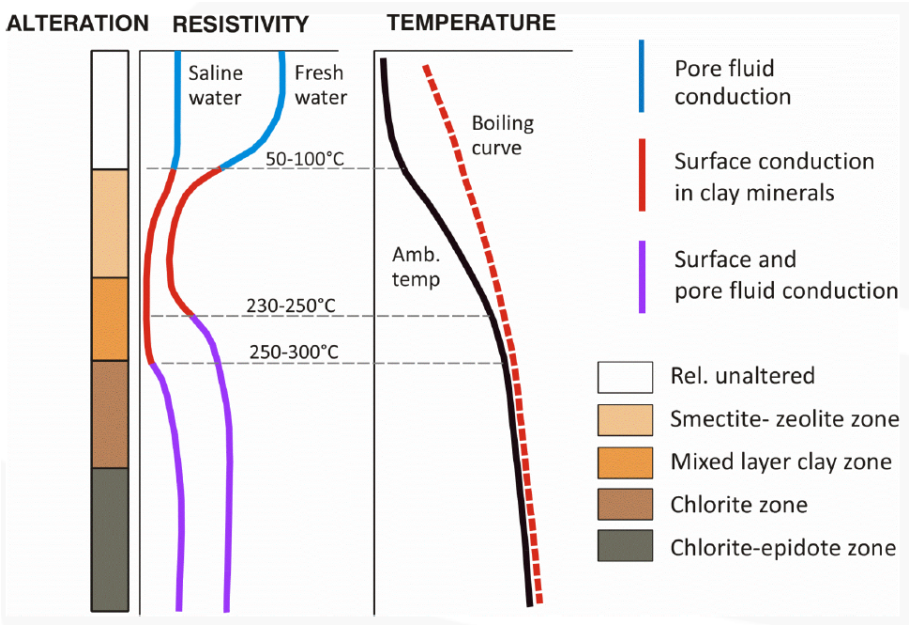

FIGURE 4: Resistivity layering of a high-temperature area (Flóvenz et al., 2012)

Although resistivity has a direct relationship with alteration temperature, it does not always present the true rock temperature of the system (Árnason et al., 2000). Resistivity sometimes shows the fossil temperature of the system, if the system is not in equilibrium with the present temperature of the system (Figure 7). Therefore, a young system may indicate lower temperature than the true high temperature in a resistivity survey. A system that has undergone cooling may on the other hand show higher alteration temperature than the true temperature. Resistivity and temperature data often indicate the system's evolution history (Figure 7) (Flóvenz et al., 2012).

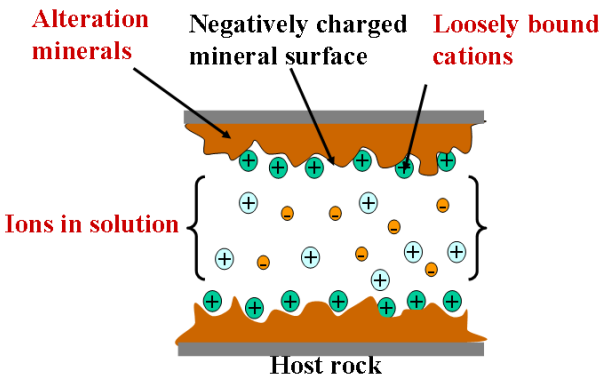

FIGURE 5: Surface conduction mechanism (Hersir, 2012)

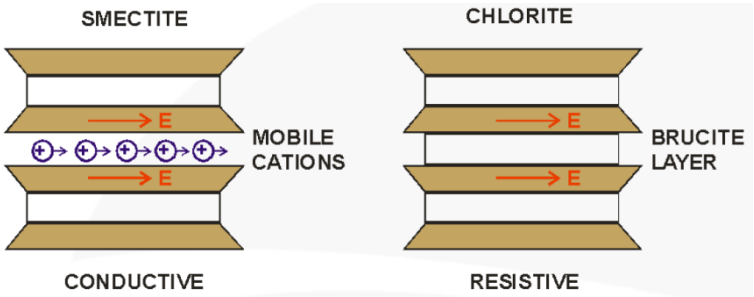

FIGURE 6: Difference between smectite and chlorite in terms of mobile cations (Hersir, 2012)

4. EM METHODS

Electromagnetic methods are particularly important as they provide reliable information on the Earth's interior. In EM methods, the measurements are done in two ways: one is time domain measurement (TEM); the other one is frequency domain measurement (FEM). The frequency of electromagnetic methods ranges widely and the resolution of data may be from a few metres to kilometres in depth. One can carry out an electromagnetic survey with or without a controlled source. Common types of electromagnetic methods used in geophysical survey are (Kearey et al., 2002):

1) Ground Penetrating Radar (GPR)
2) Very Low Frequency (VLF)
3) AFMAG (Audio Frequency Magnetics)
4) TEM (Transient ElectroMagnetics)
5) MT (MagnetoTellurics)
6) EM

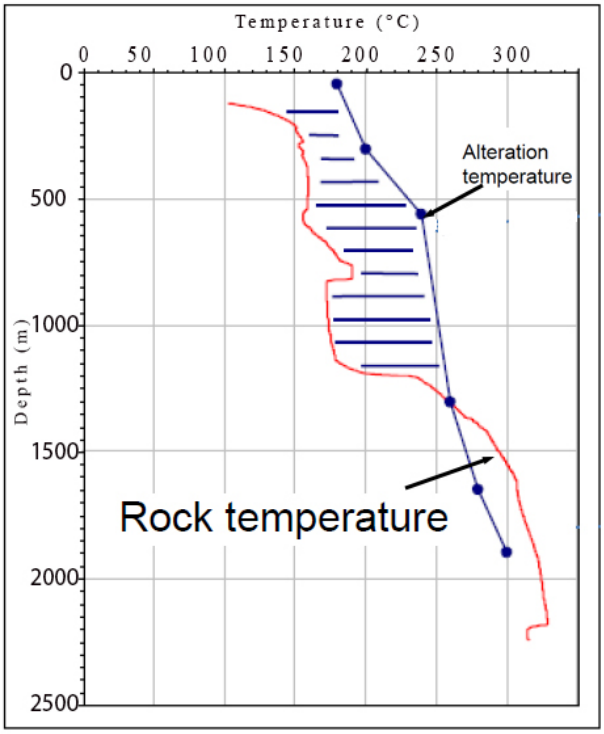

FIGURE 7: Temperature curve from a young geothermal system in the lower part (modified from Mortensen et al., 2006)

4.1 Transient electromagnetic method (TEM)

In TEM, a constant primary magnetic field is built up by transmitting a constant current into a loop. A magnetic field is generated by switching off the current source in the transmitter loop. This magnetic field decreases when it passes through the earth. According to EM induction law, this phenomenon generates a secondary current in geological materials. The voltage of this current depends upon the strength of the primary magnetic field and the electrical properties of the materials (Figure 8):

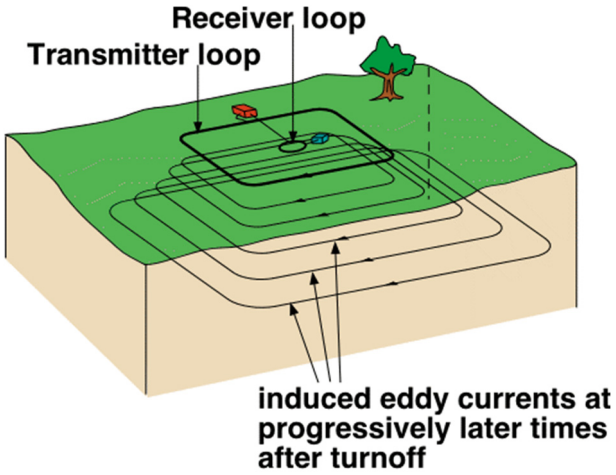

FIGURE 8: Diffusion of secondary current in TEM (modified from Rowland, 2002)

$$e(t) = \frac{k_1 M \sigma^{3/2}}{t^{5/2}} \qquad (6)$$

$$\rho_a(t) = \frac{M^{2/3} k_2}{e(t)^{2/3} t^{5/3}} \qquad (7)$$

where $e(t)$ = Output voltage from the receiver coil (V);
σ = Conductivity (S/m);
ρ_a = Apparent resistivity (Ωm);
k_1, k_2 = Constants;
t = Time (s);
M = Product of the current in the transmitting loop and its effective area.

The secondary current creates another secondary magnetic field that is measured by a receiver coil at different time gates (Figure 9). Like a bubble, the secondary magnetic field goes deeper and deeper and the voltage is measured until it is impossible to differentiate between noise and signal. Earlier time gate

readings give shallower depth information and the time span of earlier time gates are kept narrower than the late time gates which give deeper geological information (Árnason, 2006a):

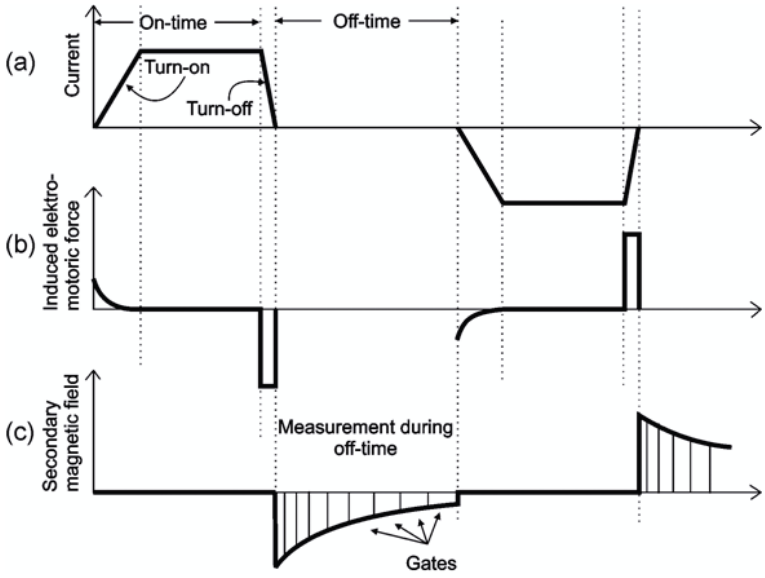

FIGURE 9: Measurement zone and time gates (modified from Rowland, 2002)

4.2 TEM for a homogeneous earth

If the earth consists of homogeneous geological material and a TEM graph is plotted with voltage on the y axis and time on the x axis, then the graph will be similar to Figure 10. It is clear from the graph that the decay of the voltage is not exponential with time at the early stage. It is happening because, at the initial stage, the secondary current is trapped beneath the transmitter coil. So there is slow change in the secondary magnetic field that gives rise to small voltage. If the early time voltages are converted into apparent resistivity, it will give higher resistivity than the true resistivity of the layer, according to Equation 7. The dash-line in Figure 10 shows what should be the early time voltage, according to Equation 6. In a two-layer case, when the resistivity of the second layer is high compared to the first layer, the decrease in voltage will be much higher at the late stage than for a single-layered earth (Figure 11). In the reverse case, when the second layer has lower resistivity than the first layer, then the voltage decrease will be slower than in the single-layered earth (Wightman et al., 2003).

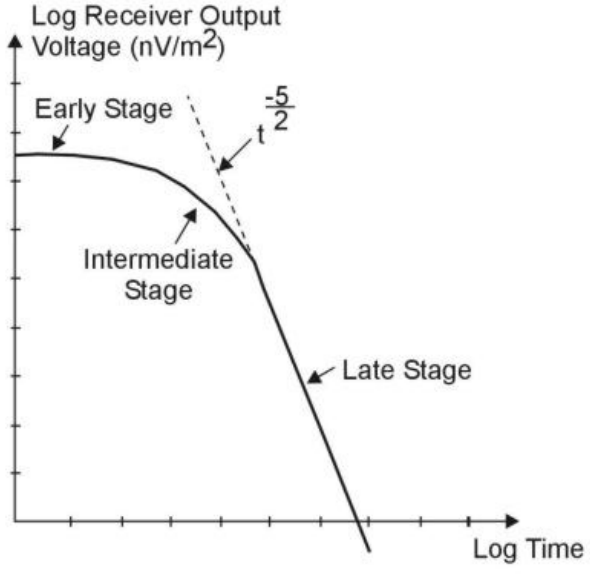

FIGURE 10: TEM response for a homogenous earth (Wightman et al., 2003)

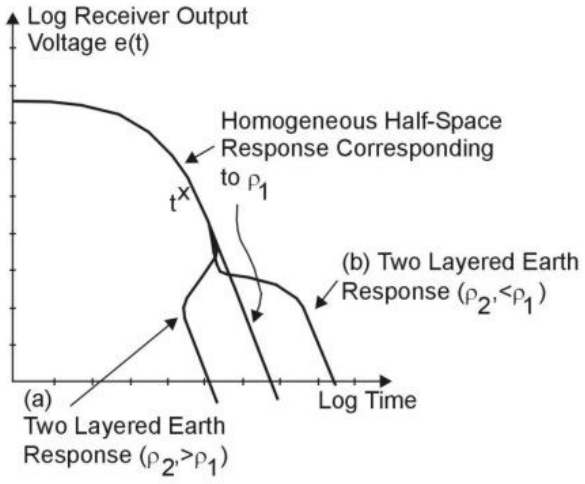

FIGURE 11: TEM response for a two-layered earth (Wightman et al., 2003)

4.3 Source for MT

MT measurements record time series of the electric and magnetic fields, generally from 0.0025 s to 1000 s. The low frequencies are generated by ionospheric and magnetospheric currents caused by solar storms

that are emitted by the sun. Their intensity has a period of 11 years. These ionospheric and magnetospheric currents, which interfere with the earth´s magnetic field, are known as micropulsations. The frequencies which are higher than 1 Hz are the causes of thunderstorm activity near the equator and travel as guided waves between the ionosphere and the earth to higher latitudes (Figure 12) (Flóvenz et al., 2012).

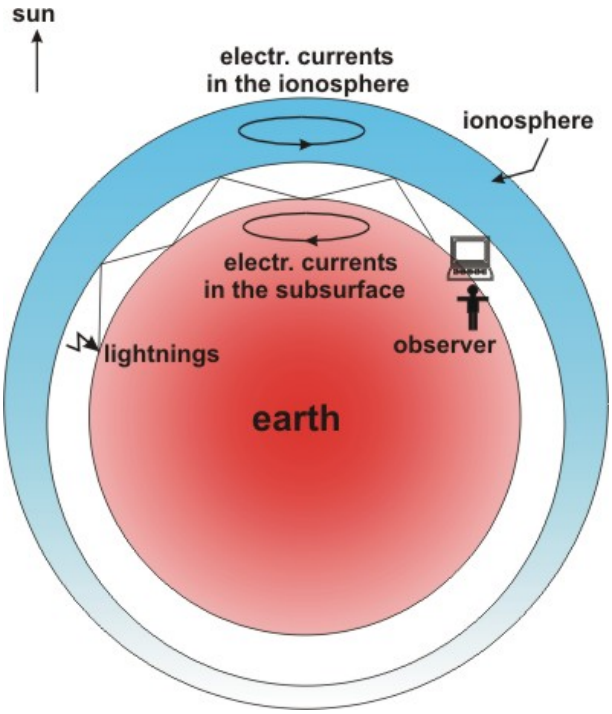

FIGURE 12: Source of MT and secondary current (modified from Freie Universität Berlin, 2008)

4.4. MT method

The magnetotelluric method is, in general, a passive method. In this method, four electrodes are used to measure the electrical field and three induction coils are used to measure the magnetic field (Tikhonov, 1950) (Figure 13). The instruments are left for one or more days in the field after being set up. The magnetotelluric method is based on Maxwell‘s equations, i.e. the electromagnetic (EM) theorems set forward in Faraday, Amper and Gauss´s laws (Equations 8, 9, 10 and 11). Since the electric field of an EM wave depends on the fluctuations of the perpendicular component of the magnetic field, the resistivity of subsurface materials is derived from the ratio of the electric field and the orthogonal magnetic field. This relationship is described by the impedance tensor (Equation 12) (Cagniard, 1953). The depth of penetration of an electromagnetic wave can be described by the skin depth, which is the depth where the electromagnetic field has decreased to 1/ e of its original value. Skin depth of an electromagnetic wave depends on its period and the resistivity of the penetrated materials (Equation 13):

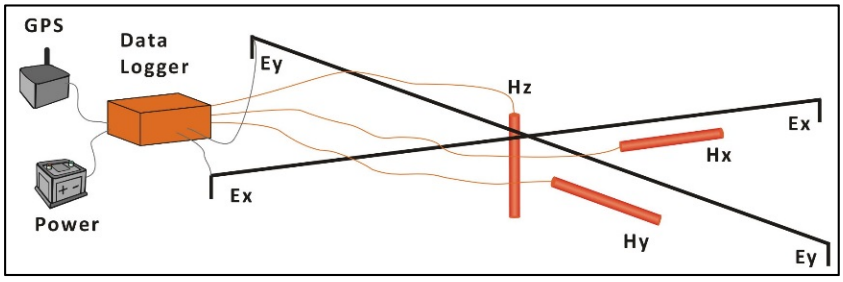

FIGURE 13: Field layout of MT (Flóvenz et al., 2012)

Faraday's law:

$$\nabla \times \boldsymbol{E} = -\mu \frac{\partial \boldsymbol{H}}{\partial t} \tag{8}$$

Ampère's law:

$$\nabla \times \boldsymbol{H} = \boldsymbol{j_c} + \frac{\partial \boldsymbol{D}}{\partial t} \tag{9}$$

Gauss's law for the electric field:

$$\nabla \cdot \boldsymbol{D} = \eta \tag{10}$$

Gauss's law for the magnetic field:

$$\nabla \cdot \boldsymbol{B} = 0 \tag{11}$$

The *apparent resistivity* derived from Maxwell's equations:

$$\rho_{xy} = 0.2T\left|Z_{xy}\right|^2 = 0.2T\left|\frac{E_x}{H_y}\right|^2 \quad and$$
$$\rho_{yx} = 0.2T\left|Z_{yx}\right|^2 = 0.2T\left|\frac{E_y}{H_x}\right|^2 \tag{12}$$

Depth of penetration of EM wave (m):

$$\delta(T) = 500\sqrt{T\rho_a} \tag{13}$$

where $\boldsymbol{E}$ = Electric field (V/m);
$\boldsymbol{H}$ = Magnetic intensity (A/m);
$\boldsymbol{D}$ = Electric displacement current (C/m^2);
$\boldsymbol{B}$ = Magnetic induction (T);
μ = Magnetic permeability (H/m);
E_x = Electrical field in x direction;
$\boldsymbol{j}$ = Electrical current density (A/m^2);
ε = Electrical permittivity (F/m);
δ = Skin depth (m);
T = Period (s);
ρ_a = Apparent resistivity (Ωm);
H_y = Magnetic intensity in y direction;
Z_{xy} = Impedance tensor element for the electrical field in x direction and the magnetic field in y direction;
ρ_{xy} = Apparent resistivity related to the electrical field in x direction and the magnetic field in y direction.

4.5 MT impedance tensor and dimensionality

Using Maxwell's equations (Equations 8-11), the following relation can be derived:

$$\begin{bmatrix} E_x \\ E_y \end{bmatrix} = \begin{bmatrix} Z_{xx} & Z_{xy} \\ Z_{yx} & Z_{yy} \end{bmatrix} \begin{bmatrix} H_x \\ H_y \end{bmatrix} \tag{14}$$

Furthermore, we have:

$$Z_B = \frac{Z_{xy} - Z_{yx}}{2} \tag{15}$$

$$Z_{det} = \sqrt{Z_{xx}Z_{yy} - Z_{xy}Z_{yx}} \tag{16}$$

$$Z_{gm} = \sqrt{-Z_{xy}Z_{yx}} \tag{17}$$

For the skew:

$$S = \frac{Z_{xx} + Z_{yy}}{Z_{xy} - Z_{yx}} \tag{18}$$

And for the Tipper:

$$H_z = T_x H_x + T_y H_y \tag{19}$$

The phase is given as:

$$(\theta_{ij}) = tan^{-1}\left(\frac{Im\{Z_{ij}\}}{Re\{Z_{ij}\}}\right) \quad (20)$$

And finally the determinant value of the apparent resistivity:

$$\rho_{det} = 0.2T|Z_{det}|^2 \quad (21)$$

where Z_{xx}, Z_{yy}, Z_{xy} and Z_{yx} = The impedance tensor elements;
S = A 3D indicator, the Skew;
Z_B = The arithmetic mean of the impedance tensor;
Z_{det} = The determinant of the impedance tensor;
Z_{gm} = The geometric mean of the impedance tensor;
T_x and T_y = The x and y components of the Tipper; and
ρ_{det} = The determinant value of the apparent resistivity.

For 1D earth $Z_{xx} = Z_{yy} = 0$ and $Z_{yx} = -Z_{xy}$; therefore, $\rho_{xy} = \rho_{yx}$ and $Z_B = Z_{det} = Z_{gm}$.

In 1D earth the resistivity in the x and y directions will be same. But in reality, the earth is not 1D. Therefore, the variation in resistivity is not in one direction only. In 2D earth, the resistivity variations are in the vertical direction and in one horizontal direction. The horizontal direction perpendicular to that direction is generally called the electrical strike direction. Along this direction there will be no variation in resistivity in the horizontal direction. This direction (Zstrike) can be found by rotating the impedance tensor elements mathematically by minimizing its diagonal elements (Z_{xx}, Z_{yy}). The electrical strike direction generally coincides with the geological strike direction. The electrical strike direction is a function of the frequency and varies therefore with depth. But, in most cases, it is not easy to find the electrical strike direction, due to the 3D nature of the earth. Zstrike has a 90° ambiguity problem which can be resolved by using the Tipper strike (Equation 19).

In 1D earth, Z_B, Z_{det} and Z_{gm} are equal; and in a 2D earth, Z_{det} and Z_{gm} reduce to the same value but Z_B is different (Equations 15-17). For a 3D earth, all three parameters are different. Skew also indicates the dimensionality of the earth: if it has a value close to zero, it indicates 1D or 2D earth (Equation 18). If the earth is not 1D, it is customary to invert for the determinant value of the tensor, the determinant value of resistivity and phase (Equation 21) (Flóvenz et al., 2012).

4.6 MT response for layered earth

For two layers, the impedance tensor at the surface of the earth is given by:

$$Z_{xy} = \frac{E_x}{H_y} = \frac{i\omega\mu}{k_1}\frac{(k_1 + k_2)e^{2k_1h} + (k_1 - k_2)}{(k_1 + k_2)e^{2k_1h} - (k_1 - k_2)} \quad (22)$$

where k_1 = Wave number diffused into first layer;
k_2 = Wave number diffused into second layer;
μ = Magnetic permeability (H/m);
h = Thickness (m);
ω = Angular frequency; and
i = Complex entity.

According to Equation 22, the apparent resistivity will be equal to the resistivity of the first layer for high frequency and equal to the resistivity of the second layer for low frequency. If a two-layer model is considered for 10 Hz, 0.1 Hz, and 0.01 Hz, then the response should be similar to Figure 14. When the resistivity increases with depth, the phase is less than for a homogeneous earth (π/4) and, if it decreases with depth, the phase will be higher than for a homogeneous earth (π/4) (Unsworth, 2012).

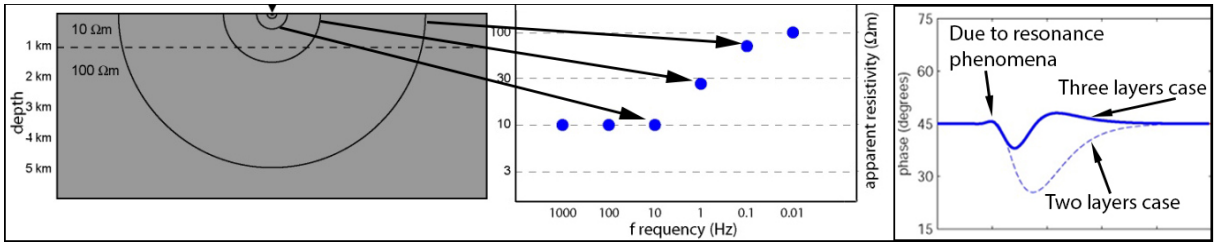

FIGURE 14: Two-layered earth and its response (modified from Unsworth, 2012)

4.7 Static shift problem

The MT method, like vertical electrical soundings, suffers a static shift problem. In static shift, the whole response of the Earth is shifted downward or upward, thereby giving misleading resistivity and depth values. This shift is called static shift because it affects all the data in the same way. The phenomenon of static shift does not affect the phase of the MT impedance tensor. This shift is independent of frequency in MT surveys. Static shift is a big problem where the change in resistivity is abrupt rather than gradual, especially in volcanic areas, and it creates severe problems for MT soundings (Jones, 1988; Sternberg et al., 1988; Árnason, 2008).

Static shift occurs for two reasons:

Current distortion: A shallow buried body may cause current distortion or current channelling (Figure 15). The body distorts the magnetotelluric apparent resistivity data.

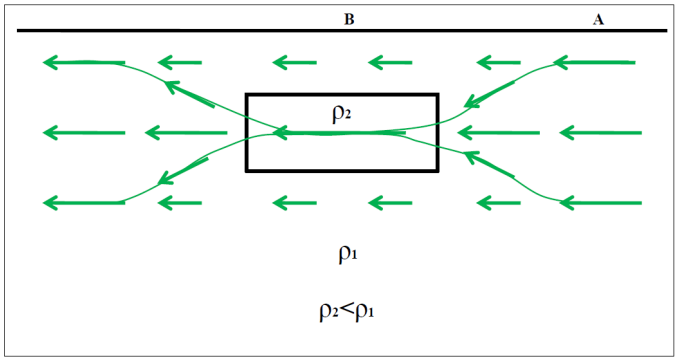

FIGURE 15: Current channelling (Árnason, 2008)

Electric field distortion: This distortion occurs because of vertical resistivity inhomogeneity. The electric field is higher in the resistive region due to the slow passage of current which increases the voltage over the resistive zone. If a geological material that is very thin and localized has high conductivity, then all the layers below it will be moved upward (Figure 16). In another case, if a localized layer has low conductivity then all the layers move downwards (Figure 17).

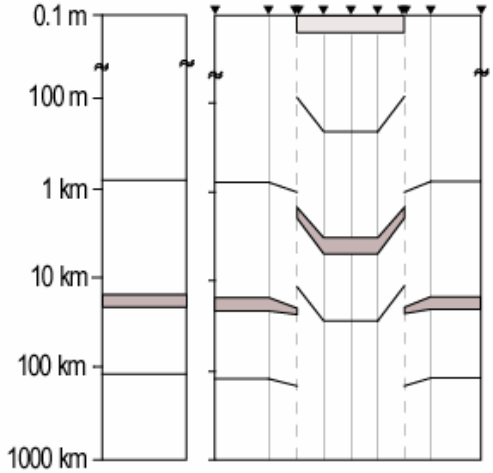

FIGURE 16: Layers move upwards due to a near-surface conductive body (Stephen et al., 2003)

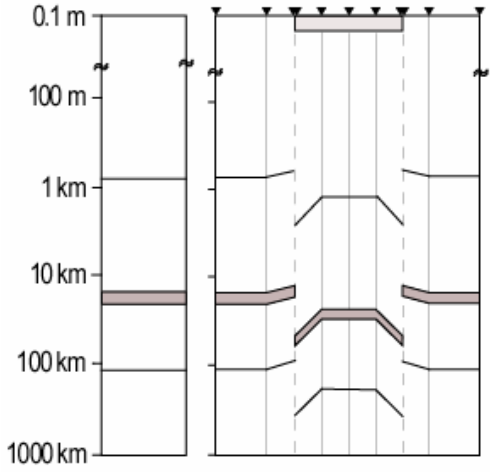

FIGURE 17: Layers move downwards due to a near-surface resistive body (Stephen et al., 2003)

From Figures 16 and 17, it is also clear that the MT data suffer maximum distortion at the boundary of an anomalous zone (Stephen et al., 2003).

5. FIELD PROCEDURE AND DATA ACQUISITION

5.1 Field procedure of TEM

Site selection: Before setting up a TEM measurement, the geophysicist has to select a suitable square place within the desired area. A good idea is to view the selected area through Google Earth or some other satellite images. The area should be as free from electrical noise as possible, more or less flat, and it should also not be disturbed by mechanical vibrations.

Instruments: Iceland GeoSurvey (ISOR) generally uses GEONIC´s Protem transmitter and receiver with an extra receiving antenna which has an effective area of 5613 m^2 (Figure 18). The different components of the TEM instrument are:

1) Generator (5kW),
2) Receiver,
3) Transmitter,
4) Power module for boosting current,

Receiver (Protem)

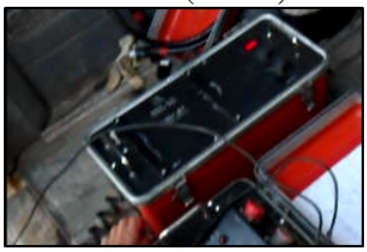
Power Booster


Transmitter


Field set up of Large Receiver coil (10 x10 m, efective area of 5613 m^2)


Small Receiver coil (100 m^2)


Connection of larger Coil with the Instrument

FIGURE 18: Setup of instruments in the field: Receiver (Protem), Power booster, Field setup of the large receiver coil (10x10 m, effective area of 5613 m^2), Transmitter, Small receiver coil (100 m^2), Connection of larger coil to the instrument.

5) Electrical wire (1200 m) for laying out the transmitting loop,
6) Clinometer,
7) Receiver coils (100 m^2 & 5613 m^2),
8) GPS,
9) Reference cable (for reference mode).

Synchronization: It is not necessary to synchronize the atomic clocks in the receiver and transmitter during TEM measurements in reference mode. The main disadvantage of the reference mode is that the size of the transmitter loop should be based on the length of the reference cable. But in synchronization mode, one can lay out any size of transmitter loop based on the available electrical wire and desired depth. In synchronization mode, it is necessary to synchronize the transmitter and receiver before making a measurement. The crystals clocks in both the transmitter and the receiver must be heated for half an hour or more and synchronized before doing the measurement. During that time, the crew can lay out the transmitter loop.

Field layout: Field layout of a TEM sounding is very simple. Generally, a transmitting loop of square shape is made, the size of the sides based on the depth of investigation. For 1000 m penetration depth, a 300 m × 300 m transmitter loop is suitable. The centre of the loop has to be marked for locating the receiving coil. After completion of field layout, the current in the transmitter loop and the turn off time are measured.

Measurement of current and turn off time: Current from the transmitter is injected into the transmitting loop. It is measured at low frequency (2.5 Hz) and the unit is Ampere. An extra power module is always used with the transmitter to increase the output current. The current value should be registered when the transmitter reading is stable. Turn off time (TOT) is measured at high frequency (25 Hz) and the unit is in micro-seconds.

Calibration and insertion of field parameters: Before performing the measurement, the receiver should be calibrated, which is done internally and automatically by the instrument itself. The area of the transmitter loop, turn off time and current value are inserted into the receiver before making the measurement.

Measurements: After inserting the TOT, current and doing the necessary calibrations, the instrument is ready for measurement. The receiver also has to set up appropriate gain and integration values, as needed. It is necessary to give unique names to each sounding. The receiver should collect 10 sets of data for each sounding which can be used later to improve data quality by stacking. The data are collected at two frequencies, the first at 2.5 Hz and the second at 25 Hz. At 2.5 Hz, both 100 m^2 and 5613 m^2 effective area receiving loops are used. At 25 Hz, only the 100 m^2 effective area loop is used. During the measurement, data should be checked on the display. If the change of the apparent resistivity value is not gradual, then the connections and inserted parameters in the receiver should be rechecked.

After the measurement, the instrument drift between receiver and transmitter is registered and used in the processing of the data.

5.2 Field procedure of MT

Similar to TEM, the MT site selection is very important. The conditions needed in TEM are also needed for MT. Figure 19 shows the field layout.

Instruments: ÍSOR generally uses the Canadian made Phoenix MT instrument. The equipment has the following components:

FIGURE 19: Field layout for MT measurements, a) Setup of true North direction; b) Adding bentonite to the electrode; c) Adding saltwater into the hole; d) Making a hole; e) Placing the vertical induction coil; f) Placing the horizontal induction coil; g) Placement of GPS; h) Instrument connection with the battery

1) Recording unit,
2) Battery,
3) Real time GPS,
4) Five non-polarizing electrodes,
5) Three induction coils,
6) Co-axial cables for connecting,
7) Four sticks,
8) Clinometer, magnetic compass,
9) Three centre-bubble level,
10) Augur and earth excavator,
11) Plastic bag,
12) GPS.

Site selection: A square-shaped area is selected with sides that are at least 50 m long. Four directions, magnetic north-south and magnetic east-west, are found with high accuracy using a magnetic compass and a spirit level. From the centre of the area, four sticks should be placed several m away in each direction.

Setup of the electrodes: Four especially made electrodes are used to measure the electrical potential for calculating the electrical field. Four holes, 40 cm deep each, are dug 25 m away from the centre in each direction. Before placing the electrodes into the holes, a small amount of salt water is poured into the hole and the bases of the electrodes are covered by bentonite clay to increase the contact of the ground with the electrodes. Four co-axial cables connect the north, south, east and west indication knobs in the instrument with the electrodes in each direction. The metallic shield of the co-axial cables is grounded with the grounding of the main instrument. A small amount of soil should be placed at regular intervals on the cable to decrease the vibration of the cable, due to wind or any mechanical movement. During layout of the wires, particular care must be taken to ensure that the co-axial cable does not make a

circular loop between the electrodes and the instrument, because this would cause induction and decrease data quality. Before making the connection of the electrodes with the instrument, the self-potential difference between each pair of electrodes should be measured; the acceptable value should be less than 25 mV.

Setup of the induction coil: Three induction coils are generally used to measure the magnetic field. Each induction coil is about 1.3 m long. A coil is placed between an electrode and the centre of measurement. Two coils must be buried horizontally, one in a magnetic North-South direction and the other one in a magnetic East-West direction. The third coil is buried vertically. To place the induction coils in true horizontal and vertical configurations, centre-bubble levels are used. Three co-axial cables are connected to each induction coil and to the recording instrument by a special connector, having indications for North, East and vertical.

Setup of the receiver: After connecting the acquisition unit to the 12 V battery, the real time GPS, non-polarized electrodes, induction coils and grounding the instrument, a 512 MB or larger memory card is inserted into the instrument; then it is ready for data acquisition. The instrument is generally placed inside a plastic bag for protection from rain. After making all the connections, the power switch of the instrument is turned on. At first it will search for satellites. The search for satellites is indicated by the quick blinking of the RED LED bottom. When it finds the satellites, the blinking will take a longer time. The instrument is left for two days or more to record data. After two days, the whole setup is removed and data can be downloaded into a laptop for processing.

6. PROCESSING AND INVERSION OF TEM AND MT DATA

6.1 Inverse theory

Inverse theory is about deriving the properties of remote objects without physical contact. Using this theory, scientists generally make inferences about the remote body. So the inference of a body is statistical, not practical. Statistically, inferences may be right but are not always true to case. The main disadvantage of inverse modelling is that a field crew generally records noisy data and these noisy data may have more than one perfect model. But the inversion of any data represents a model which is statistically correct; moreover, inversion is done using a continuum of equation. In nature, lots of factors work together that may not be truly related to only one continuum of equation. To become quantitatively correct, any model must answer three essential questions: How much data are free from noise? How much correct synthetic data can the continuum equation derive from the assumed model? How much information is available about the true object that is independent of the synthetic data? This independent information will help to separate a reasonable model from unreasonable models. The inversions of geophysical data follow a simple flow chart. First the computer selects a model, creates the synthetic data using a continuum of equation, and compares this data with the field data. If it encounters any match within acceptable statistical limits, then it will finish the processing. If the computer does not find any match, then it will iterate the process with small changes in the selected model (Figure 20) (Scales et al., 2001).

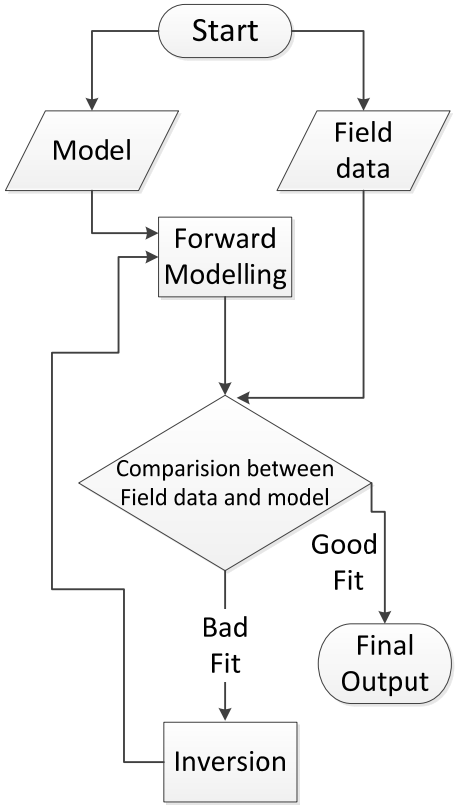

FIGURE 20: Flow chart of data inversion

6.2 Processing of TEM data

For processing TEM data, computer aid is needed. Knútur Árnason, a geophysicist at Iceland GeoSurvey (ISOR), has developed a program called TemX to process TEM data (Árnason, 2006a). The following procedures were applied to process the TEM data:

1) Sounding data were downloaded from the instrument.
2) The TemX program asked whether the data should be corrected for the turn off time as well as for drift correction. Very few data needed to be corrected. The TemX program has a GUI (graphical user interface). In the GUI, two windows can be found; one presents a voltage versus time graph and the other presents a resistivity versus time graph. There are eight buttons by which one can exaggerate or reduce the data view (Figure 21).
3) During processing, noises were identified by their offset from the trend. Generally, late time data were chosen from low-frequency data and early time data were chosen from high-frequency data. The data were masked by mouse clicking and, if needed, the data were unmasked again by mouse clicking. It is better to mask the data from the voltage plot because one can easily find ten data points at a time but, in the resistivity-plot, only the average of the data are found. After processing, the header file was edited. In the header table, elevation, location, crew´s names, place, UTM coordinates and the sounding name were inserted.
4) The file was saved later as a *.inv file which deleted the masked data that were masked during the process. The *.inv file is the final output of the TemX program and was used as an input to the TEMTD program.

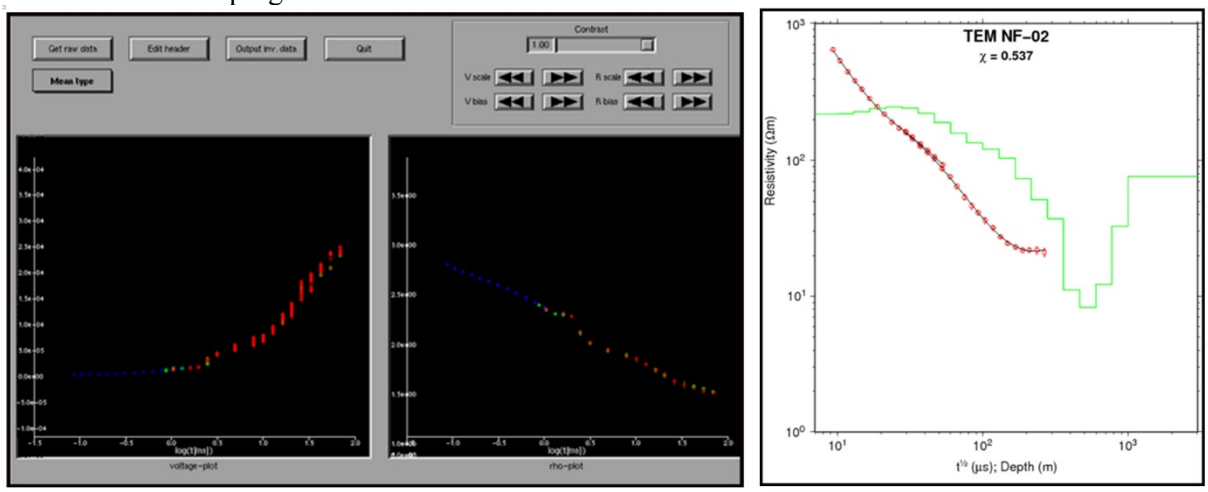

FIGURE 21: Processed TEM data to the left and the corresponding inversion of the data to the right. Left and middle panel indicate time versus voltage and time versus apparent resistivity. Blue and green circles denote data collected by the 100 m^2 loop for 25 Hz and 2.5 Hz, respectively, and red circles denote data collected by the 5613 m^2 loop for 2.5 Hz. Red (dark) circles in the right panel indicate apparent resistivity, black continuous line indicates model response and green (grey) continuous line represents the 1D inverted model. Text at the top of right panel is TEM name while the χ value represents chi misfit

6.3 1D inversion of TEM data

From Equation 6 and 7, it is clear that the response is non-linearly related to the model. For the inversion, the non-linear least-square method is used. TEMTD software was used for the inversion. In TEMTD, processed data have to be provided with a reasonable model. Then the TEMTD software inverts the data on the basis of the given model. Sometimes the inversion fails to improve the fit. This can be due to two reasons: a poor initial guess and a singularity problem. There are two types of inversions: one is simple layered earth inversion and the other is minimum structure inversion (Occam). In the Occam

inversion, the thickness of the layers remains constant. With Occam inversion, some damping factors were used to smooth the model (Figure 21) (Árnason, 2006b).

6.4 Processing of MT data

For the processing of MT data, the following operations were done sequentially after collecting data with the MT instrument:

1) In the field, the time series data were recorded and afterwards downloaded from the instrument.
2) SSMT2000 MT program from Phoenix Data Processing Software was used to convert the time series to the frequency domain. SSMT is a Windows OS based software.
3) From the Fourier transform, average cross and auto powers were calculated using the robust processing method.
4) The cross powers were then manually edited in the MTeditor program from Phoenix.
5) Then the data were saved in standard EDI file format.
6) These EDI files were the final output from the processing. EDI stands for Electrical Data Interchange, which is a universal data format for MT. Before inverting the EDI file, it was converted to UNIX format and the output of the UNIX format had an EDI extension.
7) These EDI format data were used with the TEM data for joint inversion. Figure 22 shows different parts of the MT output. The apparent resistivities are denoted by *xy* (red) and *yx* (blue); the phase also by the *xy* (red) and *yx* (blue) and the determinant invariant by black dots; Zstrike (Swift angle) also by black dots; multiple coherency by *xy* (red) and *yx* (blue), and skew by black dots and ellipticity by gray dots. The lower four graphs in Figure 22 show various forms of the Tipper data.

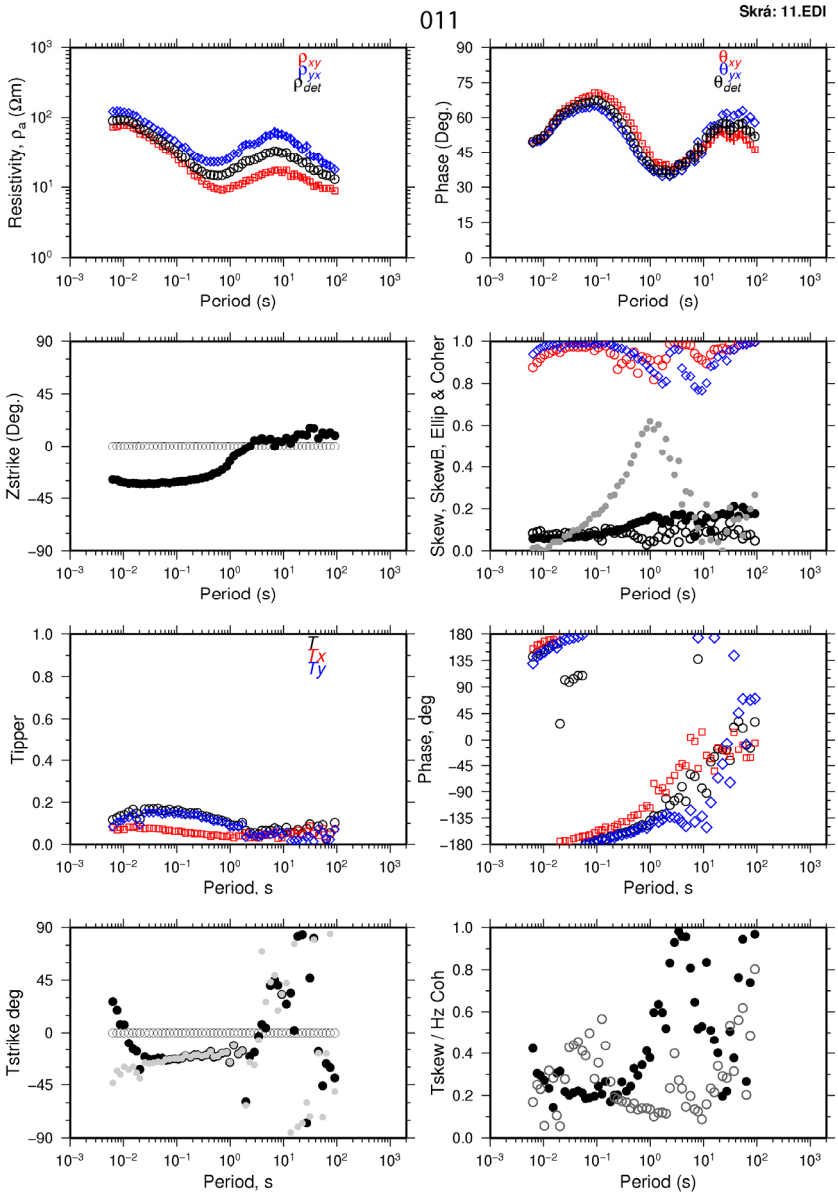

FIGURE 22: Output of MT data after processing

6.5 Joint 1D inversion of TEM and MT data

Inversion of MT data is similar to the inversion of TEM data. In this case, at first MT alone was inverted using the TEM model as an input and a model was created for joint inversion. Later, the TEM *.inv extension file was used with the processed MT data which had the same geographical position as the MT so the two types of data could be jointly inverted. In this case, a previously created MT model was used as an input model. Different attributes were used in TEMTD program to increase the match and lower the χ value (Árnason, 2006b). Red diamonds in Figure 23 are TEM apparent resistivity, blue squares and circles are the apparent resistivity and phase, respectively, derived from the determinant of the MT impedance tensor, continuous green lines in the left panel are the model response and the green curve in the right panel is the 1D joint inversion.

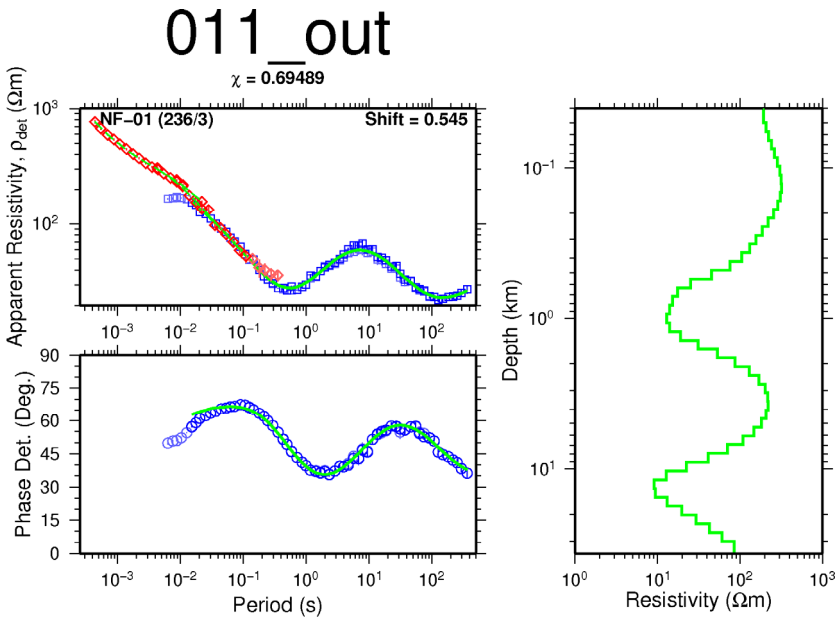

FIGURE 23: Joint inversion of TEM and MT data

7. THE NÁMAFJALL HIGH-TEMPERATURE GEOTHERMAL AREA

The Námafjall high-temperature area is located about 100 km east of Akureyri town, N-Iceland. Every year many foreign tourists visit this place. The high-temperature area is situated about 300-400 m above sea level. The soil colour of the area is brownish to yellow. Lake Mývatn and Krafla volcano are located about 5 km southwest and north of the area, respectively. The soil here is barren and no grass or trees grow due to the high temperature and acidic nature of the surface materials (Figure 24).

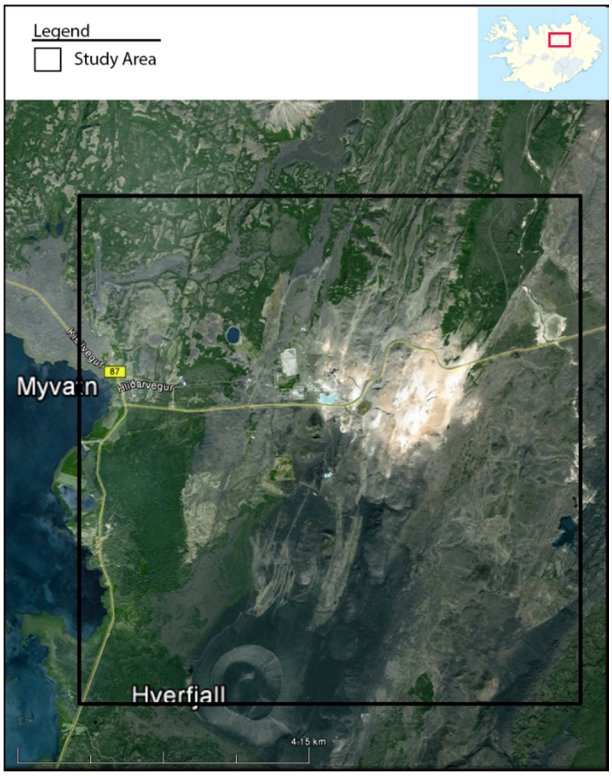

FIGURE 24: Location map of the study area (Google Earth, 2012)

7.1 Geological and structural settings of the study area

Námafjall means “mountain of the mines”. From the meaning of the name, it is clear that the area is very important from a geological point of view. Námafjall field is located on the Námafjall ridge which is about 2.5 km long and 0.5 km wide. Námafjall ridge is a part of the Námafjall-Dalfjall-

Leirhnjúkur ridge. Námafjall field is a part of the active Krafla volcanic system (Pálmason and Saemundsson, 1974), so the geology of this area is associated with the geology of Krafla. Fissure swarms, active volcanoes, numerous faults, fractures and grabens define the geology of the Krafla volcano system. Námafjall ridge itself was formed by sub-glacial eruption at the time of the last glaciation. Postglacial basaltic rock constitutes the upper part of the ridge. Two major faults/fractures, namely Krummaskard and Grjótagjá, were heavily affected during the Krafla eruptions in 1975-1984 (Figure 25). The mineralogical composition of this area is mainly plagioclase to olivine tholeiites. stratigraphic sequence can be divided into two parts: the upper part, having a thickness of 1100 m,

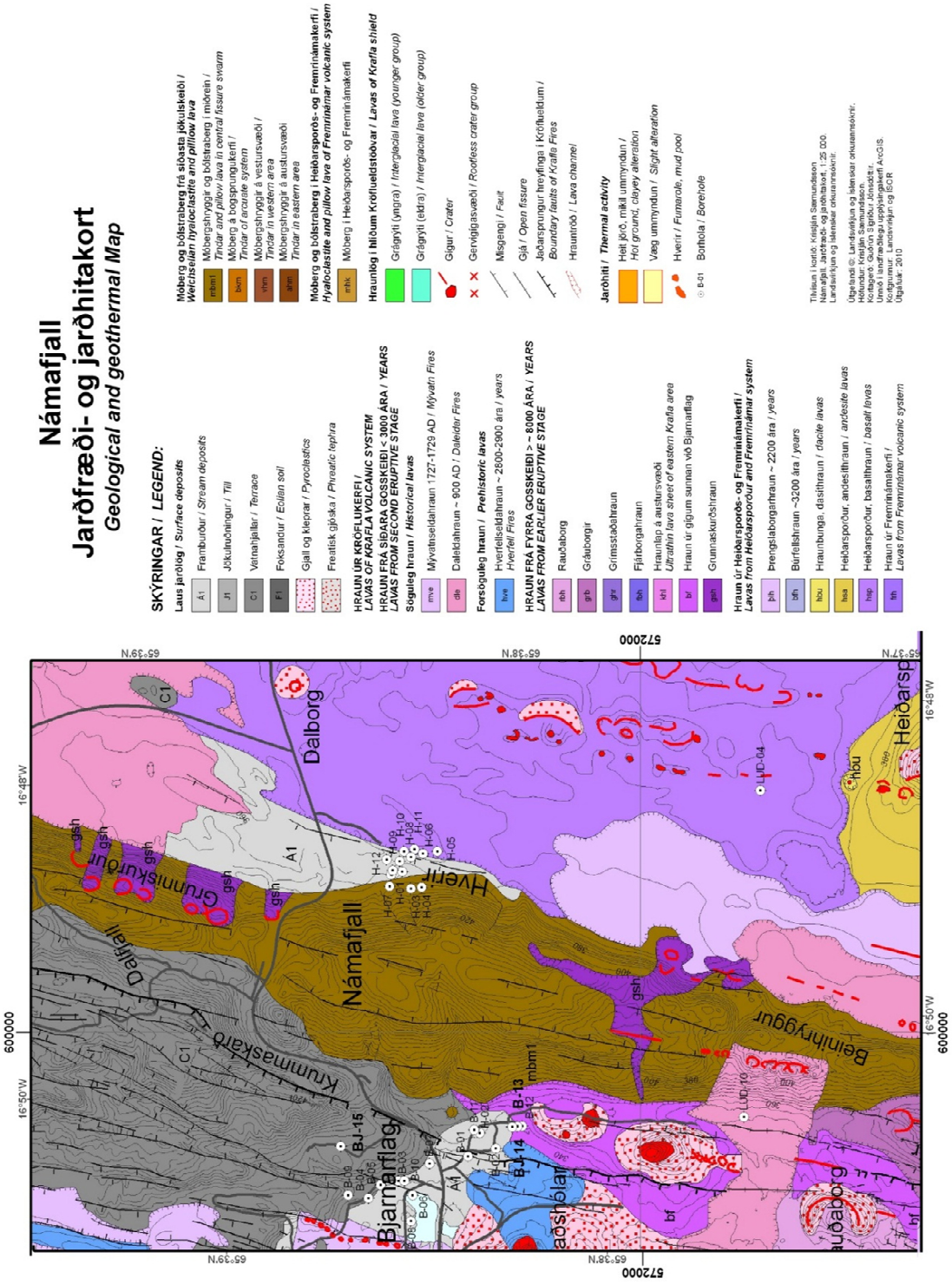

FIGURE 25: Geological map of the study area (modified from Saemundsson, 2010)

Extrusive rhyolite is also found in some places. Borehole lithological records suggest that the consists of hyaloclastites (70%) interlayered with lava, while shield volcanic eruptions with hyaloclastite constitute the main part of the lower part down to 1700 m depth. Intrusive rock units constitute about 50% of the sequence below 1700 m depth (Nicholson et al., 1991; Gudmundsson et al., 2010).

7.2 Geothermal importance of the Námafjall area

The surface indications of the Námafjall field are confined to the ridge as well as to the east and west sides of the ridge. Basically it is divided into two parts, found on each side of the volcanic ridge. The eastern part is called Hverarönd and the western part is known as Bjarnarflag. In this high-temperature area, surface manifestations are similar to that of other geothermal areas such as fumaroles and mud pots, and sulphurous odour is commonly felt (Malimo, 2012).

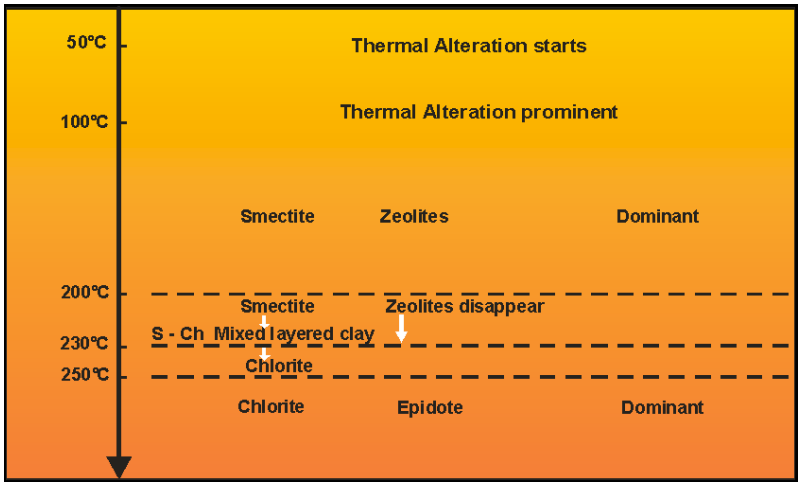

FIGURE 26: Alteration of minerals with temperature (Hersir, 2012)

Alteration in high-temperature system which is in equilibrium with the temperature of the system shows commonly known sets of alteration minerals with depth. At shallow depth where temperature is less than 100°C, fresh or unaltered rocks are found. At increasing depth, temperature generally increases and the alteration of rocks starts at 100°C. Up to about 200°C, zeolites and smectite type clays are common (Figure 26). With increasing depth and temperature when the system reaches 200-230°C, these clays begin to disappear and chloride and epidote start to form. Above 250°C, the dominant mineral composition is chlorite and epidote (Árnason et al., 2000).

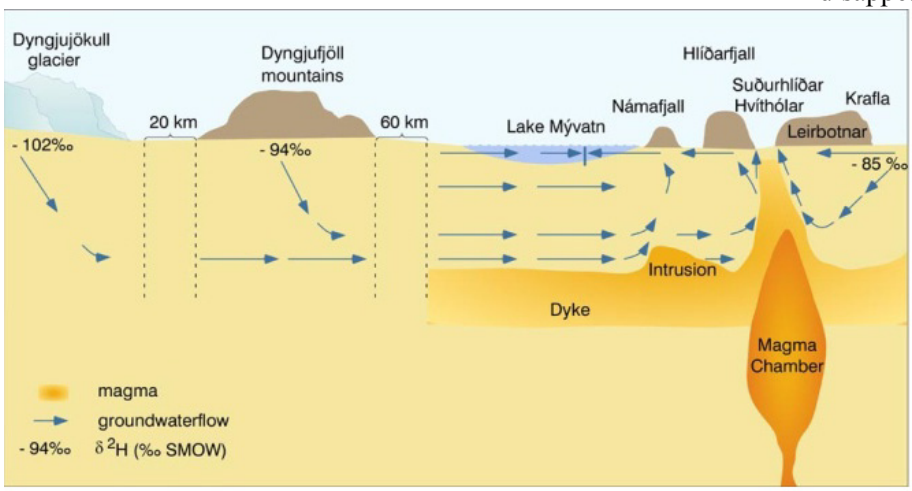

FIGURE 27: Conceptual model of Krafla-Námafjall (Gudmundsson et al., 2010)

This gradual alteration of minerals in Námafjall high-temperature area is also found in the borehole lithology of Námafjall. Although Námafjall is a high-temperature area, there are also found some low-temperature mineral assemblages together with the high-temperature minerals which indicates cooling of the field. Calcite overprinting is another evidence of cooling (Gudmundsson et al., 2010). The conceptual model of Krafla suggests that fluid is continuously extracting the heat from the underlying intrusions. The system has a good recharge of meteoritic water from outside the system's boundaries (Figure 27).

8. DATA QUALITY AND SOURCE

Due to time constraints, it was not possible to collect data from the field for study purposes. Therefore, ISOR supplied sixteen TEM and MT sounding data for the study in the Námafjall area (Figure 28). The data were collected by ISOR employees. TEM data were collected before 2001 except for one, 158771, which was collected in 2009. MT data were collected in 2009 and 2011. The TEM data are of good quality; only a few needed more than a small amount of editing. MT data are also of good quality in the middle of the frequency band, with a few exceptions, and most of them only needed editing at the beginning of the band and at the end. The interpreted TEM and MT data are presented in appendices to this report which are published as a separate report (Uddin, 2012).

The extra data needed to draw iso-resistivity maps, and to analyse static shift and the electrical strike of the area, were provided by Sakindi (2012), another UNU Fellow, who worked in the same area but with different sets of data.

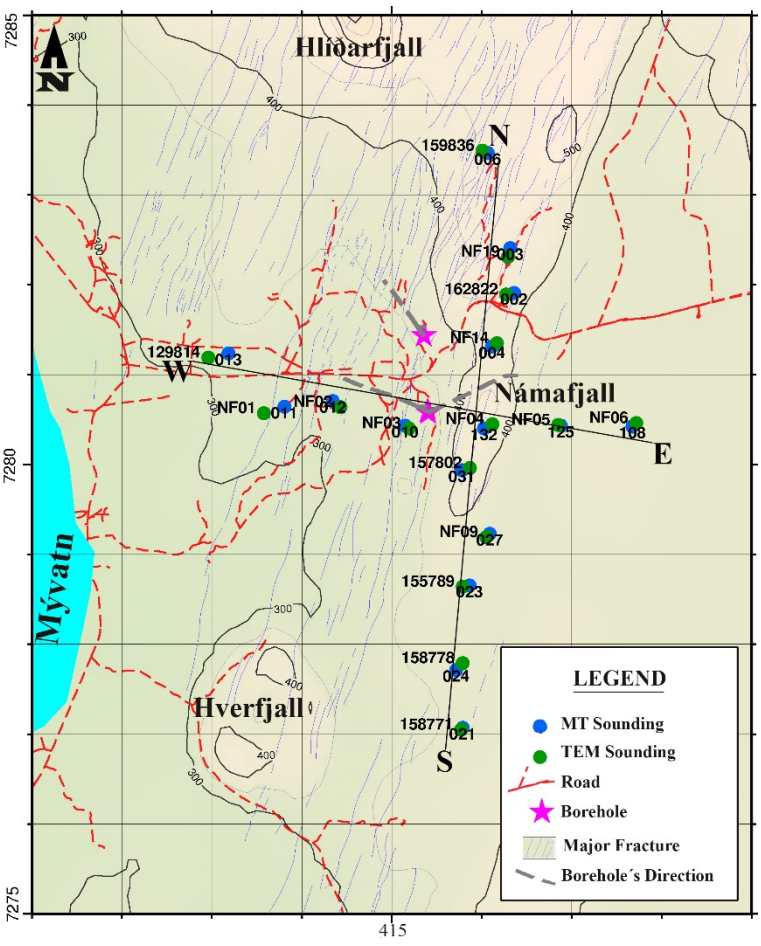

FIGURE 28: Location of MT and TEM stations, boreholes and the two resistivity profiles in the Námafjall area; pink (grey) star near MT sounding number 10 denotes borehole BJ-14 (directed to the NW) and BJ-15 (directed to the NE); the pink (grey) star near MT sounding 004 denotes borehole BJ-13

9. DISCUSSION OF INVERTED DATA

9.1 Results of TEM inversion

The 1D inversion of TEM data shows that the subsurface resistivity is not homogeneous throughout the study area and that there are large differences in the layers' resistivity. Most of the TEM inversions show that the depth of penetration was about 1000 m, except for sounding NF-06, where it was only 600 m, and they show resistivity of 20 Ωm for the bottommost layers. The rapid decrease in resistivity of the lower layer gives strong voltage for a long time; a weaker down signal was not recorded. All the inversions show that the resistivity has an increasing trend for the lowermost layer except for 5 TEM soundings: NF-06, 158771, 129814, 158778, and NF-01. The lower part of TEM sounding 162822 shows the highest resistivity, above 1500 Ωm.

All the graphs show an increase in resistivity at the lowermost part. The lowest resistivity found in the lowermost layer of sounding TEM158771 is less than 2 Ωm. Although TEM 158771 shows the lowest resistivity, it encountered this resistivity gradually; the depth of penetration at this point is about 1000 m. The top layer shows different resistivity for different soundings. All the inversions show top layer resistivity above 100 Ωm except for three soundings: NF-04, NF-05 and NF-14. NF-14 shows the

lowest resistivity for the top layer, less than 2 Ωm. But the lowest resistivity has a thickness of only 10 m and resistivity begins to increase below this layer in sounding NF-14. Soundings NF-03, NF-19, 155789, 157802, 159836 and NF-01 show a decreasing trend in the resistivity below the top layer. The rest of the soundings show an increasing trend in the resistivity (Uddin, 2012).

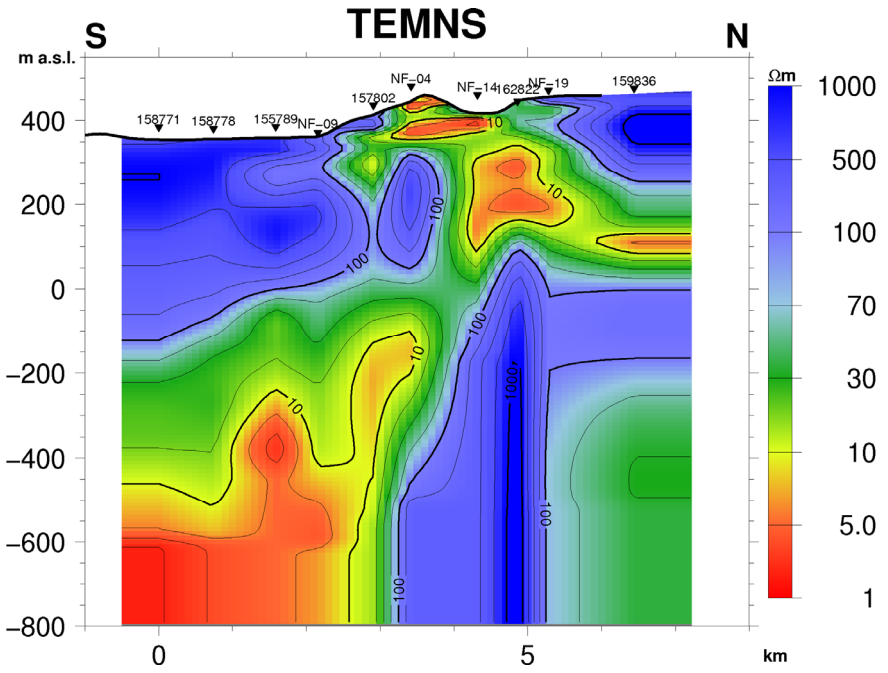

FIGURE 29: Námafjall, resistivity distribution on the N-S profile according to inversion of TEM data, down to a depth of 800 m b.s.l.

Figures 29 and 30 show the resistivity distribution of the two resistivity cross-sections, N-S and W-E (for location see Figure 28). These cross-sections were drawn, based on TEM. In the N-S cross-section (Figure 29), a low-resistivity zone can be identified that extends from the southern bottom side to the middle top. There is a conductive zone at 800 m depth which may extend to the north. The W-E cross-section (Figure 30) shows a similar resistivity distribution except the low-resistivity zone below Námafjall, which has increased in size.

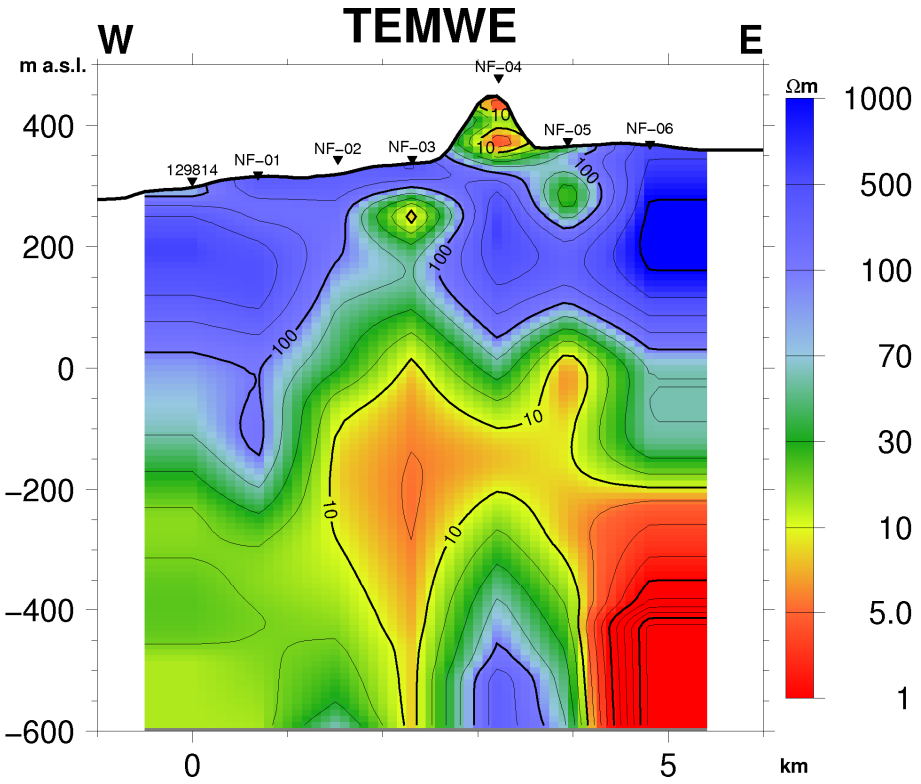

FIGURE 30: Námafjall, resistivity distribution on the W-E profile according to inversion of TEM data, reaching down to a depth of 800 m b.s.l.

9.2 Results of the joint 1D inversion of TEM and MT data

Since the resistivity distribution above 1 km has already been described in the TEM soundings, it is not necessary to repeat that description here. From the inversion of MT, it is clear that the soundings achieved a depth of penetration of more than 25 km. Below 1 km depth, the resistivity change becomes a little bit sinusoidal. This is due to the homogeneity of the materials and the change of resistivity is gradual, not abrupt. Below 1 km there are generally two resistivity maxima and one minimum in between the maxima. Below 1 km depth, the first maximum is situated between 2 and 4 km; the resistivity of this maximum varies from 50 to 100 Ωm, except for MT soundings 021, 125, and 132. The first maximum in 021, situated below 1 km depth, has resistivity of 300 Ωm. MT 125 and 132 have 20 and 40 Ωm resistivity maxima below 1 km, respectively. These first maxima can be correlated with high-temperature alteration minerals such as chlorite and epidote. One resistivity minimum is common below 1 km depth and between the two resistivity maxima. In most of the soundings, the minimum position is between 8 and 12 km depth, except for MT 132 where the minimum is not as deep, i.e. at 6 km. The resistivity values of these minima in all the soundings are less than 5 Ωm, except for MT 006, which shows a minimum value greater than 10 Ωm. The minima probably represent the heat source for the Námafjall area. All the MT soundings show a resistivity increase below 30 km depth (Uddin, 2012).

9.3 Electrical strike direction and induction arrows

To indicate the 3D nature of the electrical resistivity distribution, strike analysis was necessary. Although the geological structure is well known, Zstrike always has a 90° ambiguity problem. Resolving the 90° ambiguity problem is not always possible using some geological features (Figure 31). Some hidden geological features that have no surface expression sometimes create problems for Zstrike analysis (Flóvenz et al., 2012). Tipper analysis resolves this problem accurately. For that, the vertical component of a magnetic field should be collected during data collection. Tipper strike and Zstrike change their directions with depth on the basis of resistivity direction. Tipper strikes of 0.1-1 s and 1-100 s are shown in Figures 32 and 33. If the Tipper directions are correlated in the Námafjall area, Figure 32, then a conductive zone can be marked. Tipper directions, both in Figures 32 and 33, have a more or less similar nature; they only differ on the northern and southernmost sides. The conductive nature of Námafjall is also suggested by the resistivity value. It is interesting to point out that on the right side of Hverfjall, in Figure 33, the Tipper changed direction from northwest to northeast and, at these points, the Tipper strike subsequently changed direction. In

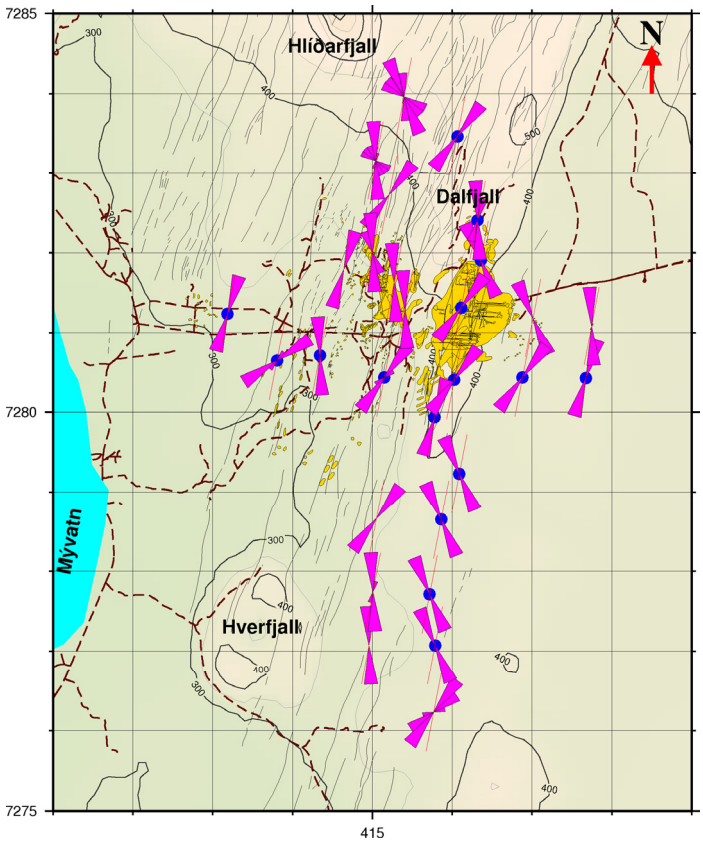

FIGURE 31: Rose diagram of Zstrike for 0.1 to 1 s; keep in mind the 90° ambiguity (see text). Blue (grey) dots are MT soundings without a vertical component of the magnetic field; roads are dark red (dark) dashed thick lines; surface manifestations are dark yellow (light grey) areas and fractures are blue (grey) thin lines

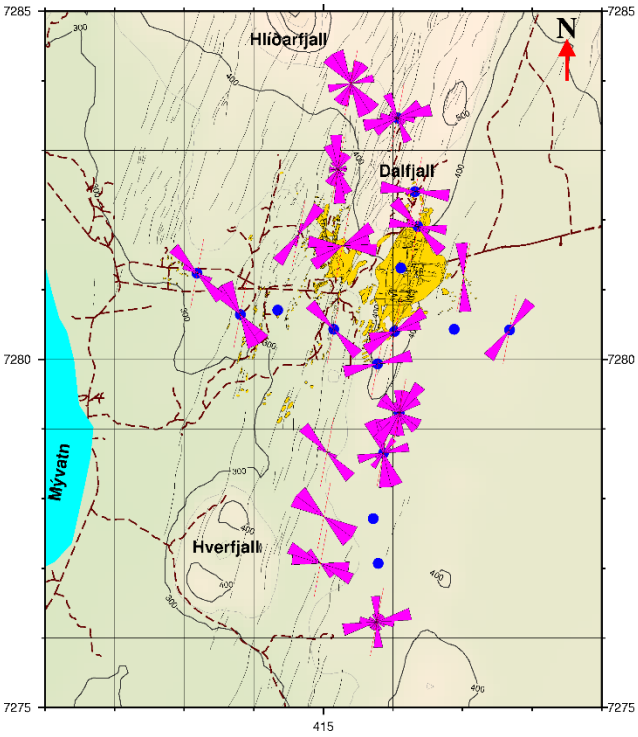

FIGURE 32: Rose diagram of Tipper for 0.1 - 1 s; symbols are explained in the Figure 31 caption

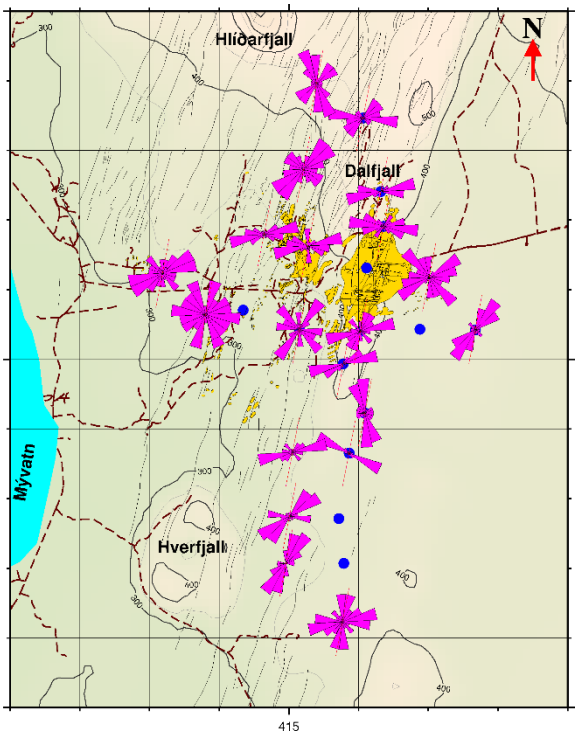

FIGURE 33: Rose diagram of Tipper for 1 - 100 s; symbols are explained in the Figure 31 caption

this area, the directions indicate a fracture zone that is oblique to the major fault. The Tipper, at very low frequency, does not follow any preferred trend.

Tipper is a complex vector. It can be represented in another way, i.e. induction arrows (Hersir et al., 2012). Induction arrows have two parts, real and imaginary. The real parts of induction arrows are represented by a blue colour and the imaginary parts by a red colour. The real parts indicate the regional variation of resistivity. On the other hand, the imaginary parts represent local variation of resistivity of the subsurface. At time period 0.1s, the imaginary parts exhibit very small magnitude compared to the real parts; most of the imaginary parts follow the same direction as the real parts (Figure 34). A conductive zone can be easily identified near the Námafjall area by the direction of the arrows pointing away from the Námafjall ridge. At time period 10 s, the local and regional influence of resistivity have become equal (Figure 35). It is very hard to find any preferred direction at subsequent time periods.

9.4 Static shift

From the histogram of static shift factor, it can be seen that the MT resistivity curves have a shift factor of both less than one, and more than one. So the MT data have suffered both downward and upward shifts. The study area has both high-resistivity and low-resistivity anomalies near the surface that have heavily distorted the electrical field. The distribution of the shift range is in the range from 0.5 to 2.5. Most of the data (16) have static shift in the range of 1-1.25. That means without static shift correction, most of the models would have shown too high resistivity and too great depths to layer's interface. This type of shift is found above fresh rocks. On Námafjall ridge and north of Hverfjall, the joint inverted data show the presence of a conductive body near the surface. Static shift above these zones is less than one. Due to this, the whole model moves upward which increases the resistivity and the depth to the layer's interface in the MT model (Figure 36).

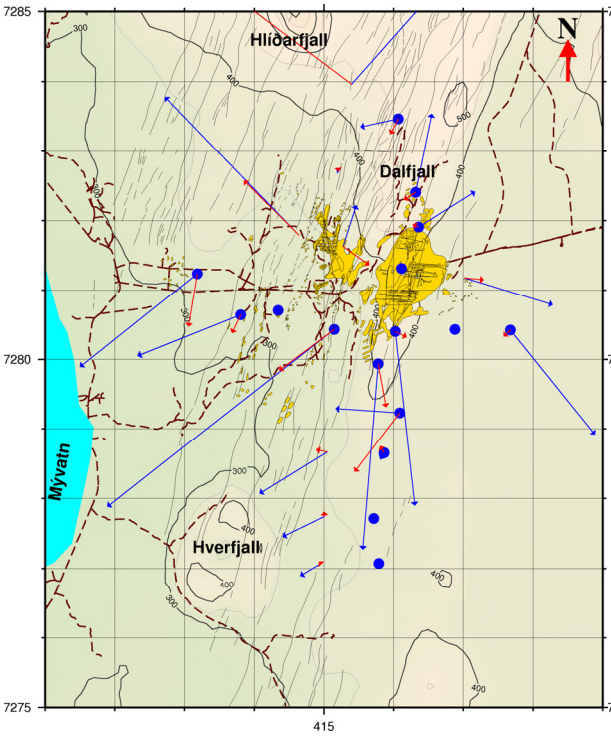

FIGURE 34: Induction arrows for 0.1 s; other symbols are explained in the Figure 31 caption

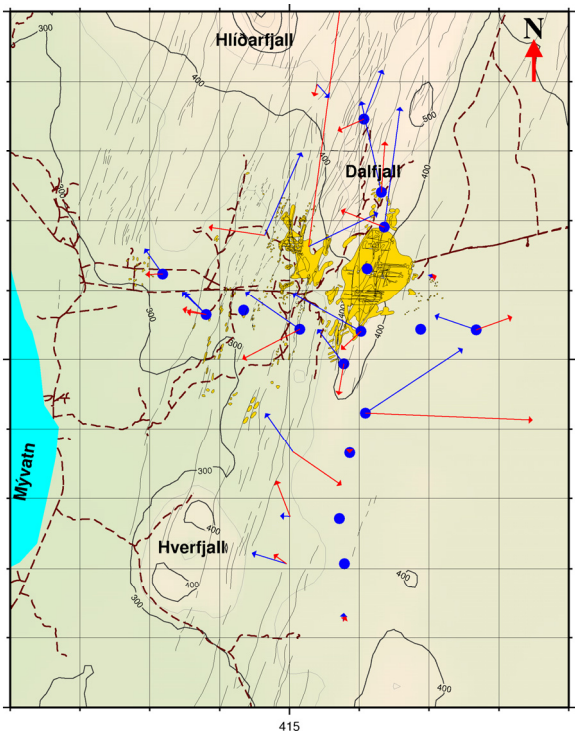

FIGURE 35: Induction arrows for 10 s; other symbols are explained in the Figure 31 caption

9.5 Interpretation of the resistivity cross-sections from joint inversion

Figures 37-40 show the resistivity distribution from the surface down to 28 km depth. Figures 37 and 38 present resistivity distribution at shallower depths down to 1000 m. In the middle of both the N-S and W-E cross-sections, a low-resistivity zone is found where values vary from 1 to 10 Ωm and which can be correlated with the low-resistivity cap. This low-resistivity cap indicates that the mineralogical compositions in this zone are mainly zeolite-smectite. The low-resistivity continuation up to the surface in the Námafjall ridge can be correlated with the surface manifestations. In the upper part of the section on both sides of the low-resistivity cap, high-resistive zones are found that reveal fresh to unaltered rock. In the lower part of these sections, the high-resistive zones are interpreted as the resistive core. The mineralogical composition of this high-resistivity core includes chlorite and epidote.

From 2000 to 14,000 m depth, both the N-S and W-E cross-sections have a similar resistivity distribution. Figures 39 and 40 show the W-E cross-section. There is a low-resistivity body in

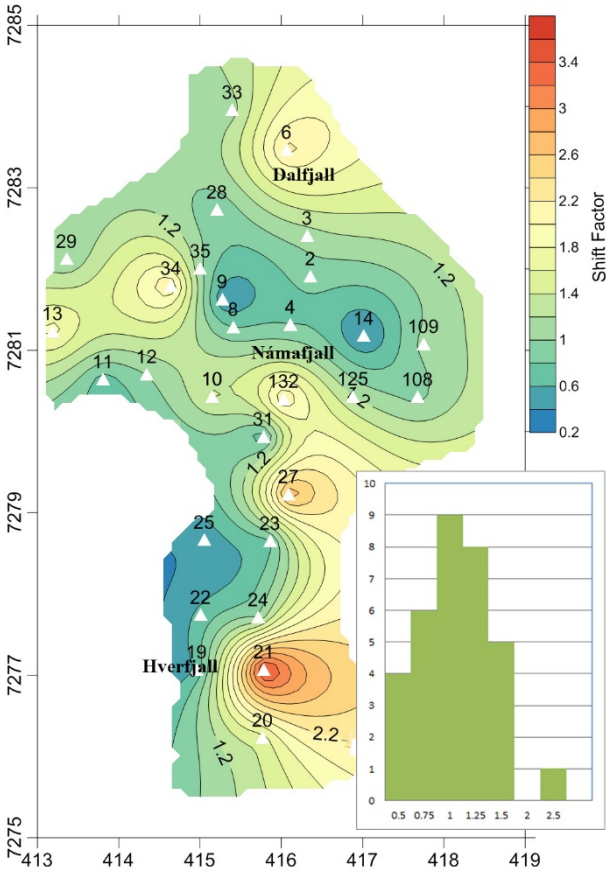

FIGURE 36: Static shift distribution and histogram of the shift factor

the middle of the cross-sections with resistivity between 1 and 10 Ωm; and on both sides of this resistivity low, there are high-resistivity zones which extend down to about 10 km. This central deep low-resistivity body shows the probable heat source for the Námafjall high-temperature area.

Below 14 km depth, the resolution of the data is poor. It is hard to infer about the nature of the resistivity distribution at greater depth (Figure 40).

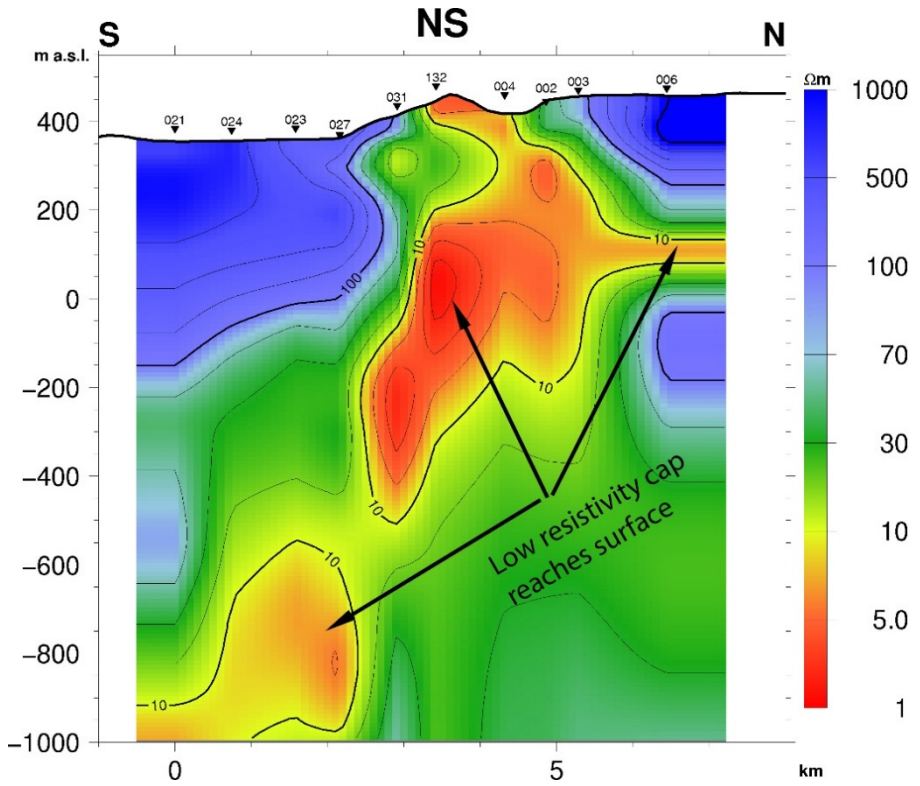

FIGURE 37: Námafjall, resistivity distribution on the N-S profile according to joint inversion of TEM and MT data, down to a depth of 1000 m b.s.l.

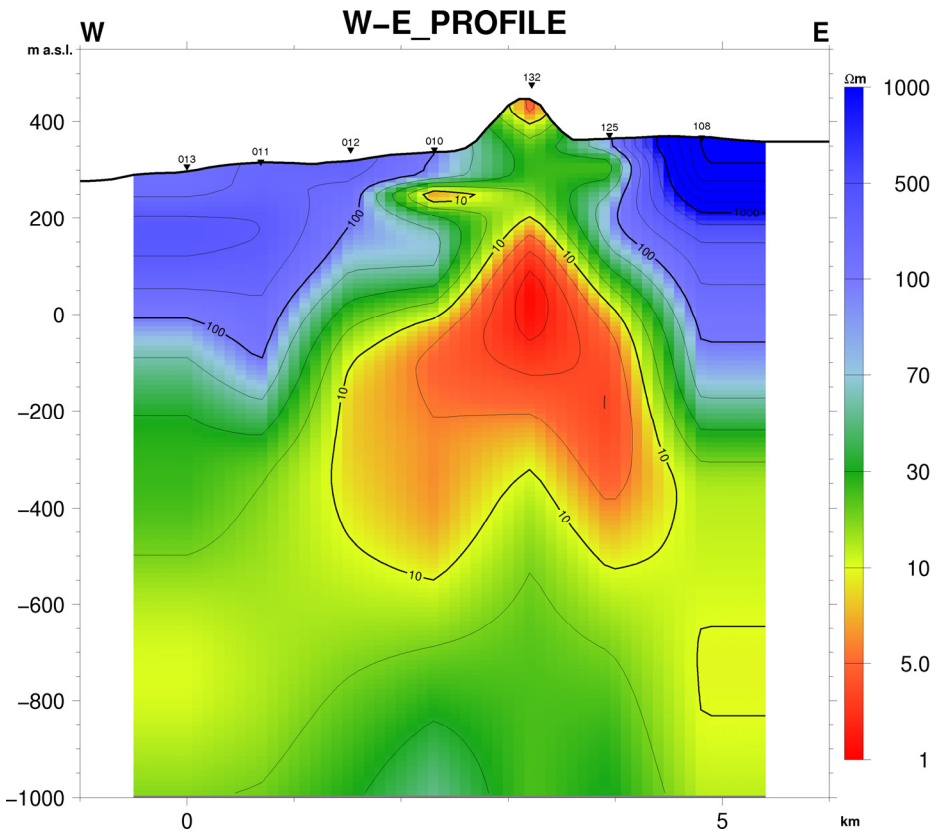

FIGURE 38: Námafjall, resistivity distribution on the W-E profile according to joint inversion of TEM and MT data, down to a depth of 1000 m b.s.l.

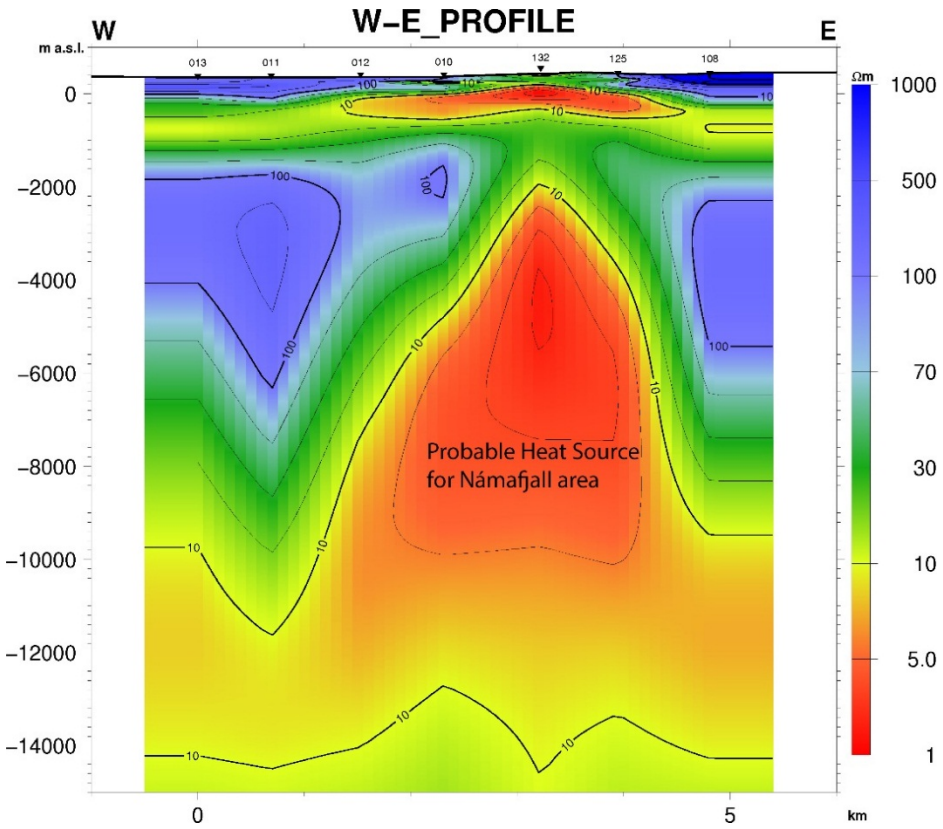

FIGURE 39: Námafjall, resistivity distribution on the W-E profile according to joint inversion of TEM and MT data, down to a depth of 15 km b.s.l.

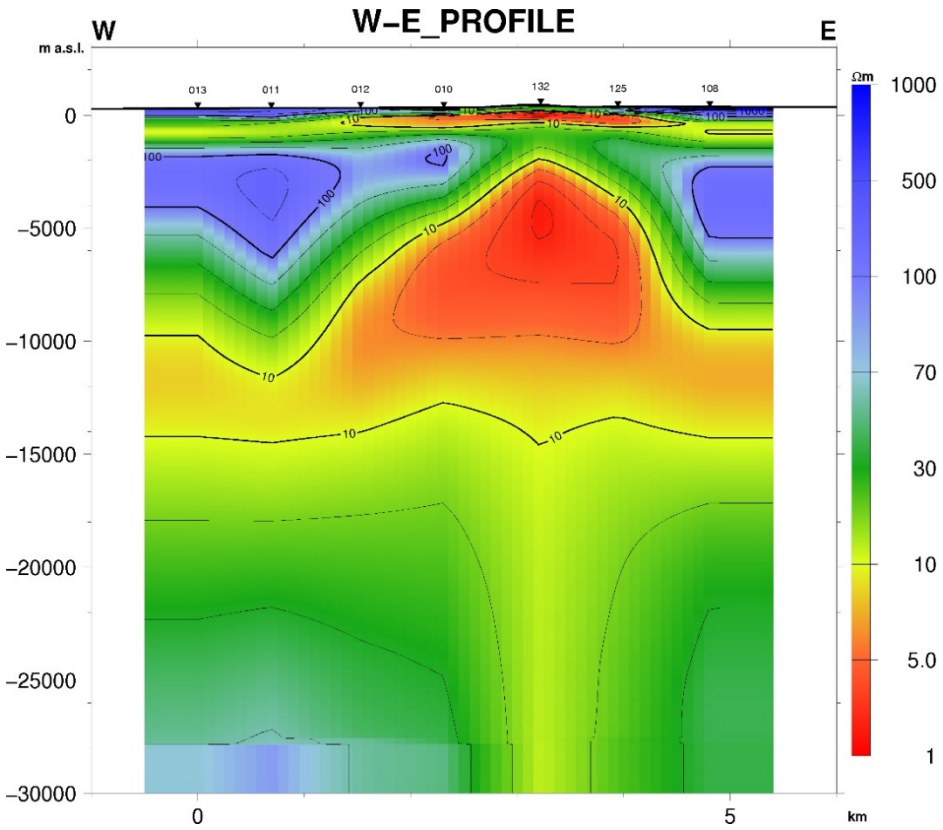

FIGURE 40: Námafjall, resistivity distribution on the W-E profile according to joint inversion of TEM and MT data, down to a depth of 30 km b.s.l.

9.6 Interpretation of iso-resistivity maps at different depths

Figures 41-46 show the resistivity distribution at +300, 0, -500, -3000, -10,000, and -20,000 m from sea level. At 300 m a.s.l., a conductive zone around the surface manifestations is found at Námafjall ridge and the rest of the areas show high resistivity around the ridge. This high resistivity indicates fresh unaltered rock. At sea level, the conductive zone has grown in size. At 500 m b.s.l. the upper conductive zone has vanished from the scenario, the resistivity distribution is similar throughout the area, and varies from 10 to 40 Ωm. The resistivity distribution signifies that the mineralogical composition at this depth is high-temperature altered minerals, mainly chlorite and epidote. At 3000 m b.s.l., another low-resistivity zone has emerged below the Námafjall area which grows in size at subsequent depth and disappears at 10,000 m b.s.l. This low-resistivity zone represents the probable heat source for the Námafjall high-temperature area. The resistivity distribution pattern below this depth is more or less uniform (Figure 46).

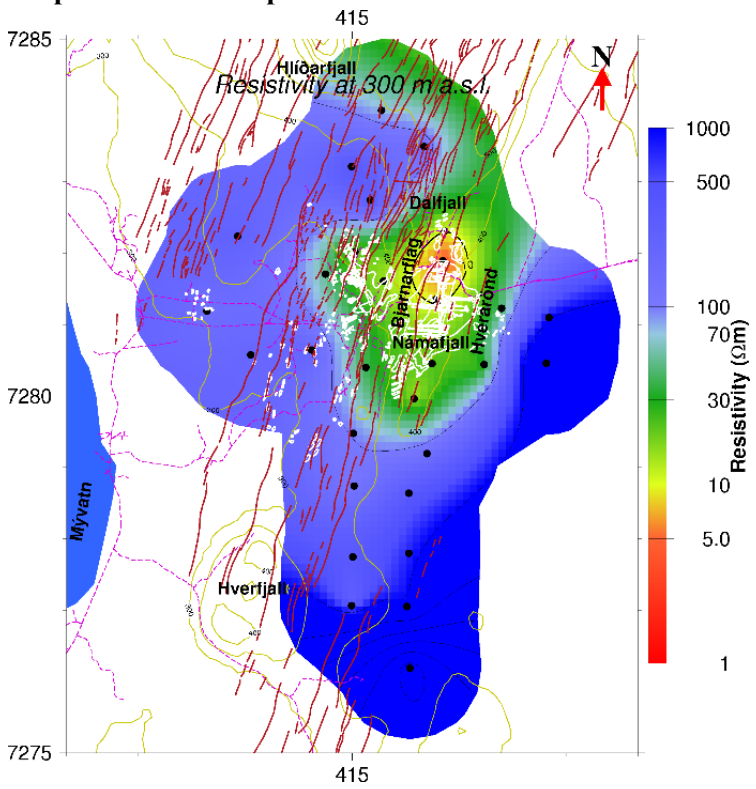

FIGURE 41: Námafjall, iso-resistivity map at 300 m a.s.l. MT soundings are denoted by black dots; fractures by magenta (dark) thick lines; surface manifestations by white spots and roads by pink (grey) dashed thin lines

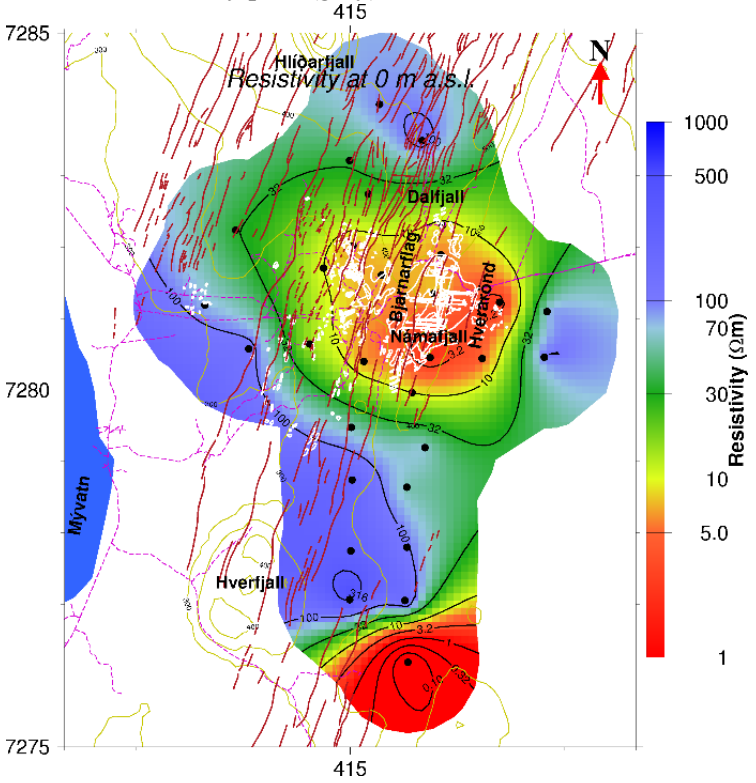

FIGURE 42: Námafjall, iso-resistivity map at 0 m a.s.l.; symbols are explained in the caption of Figure 41

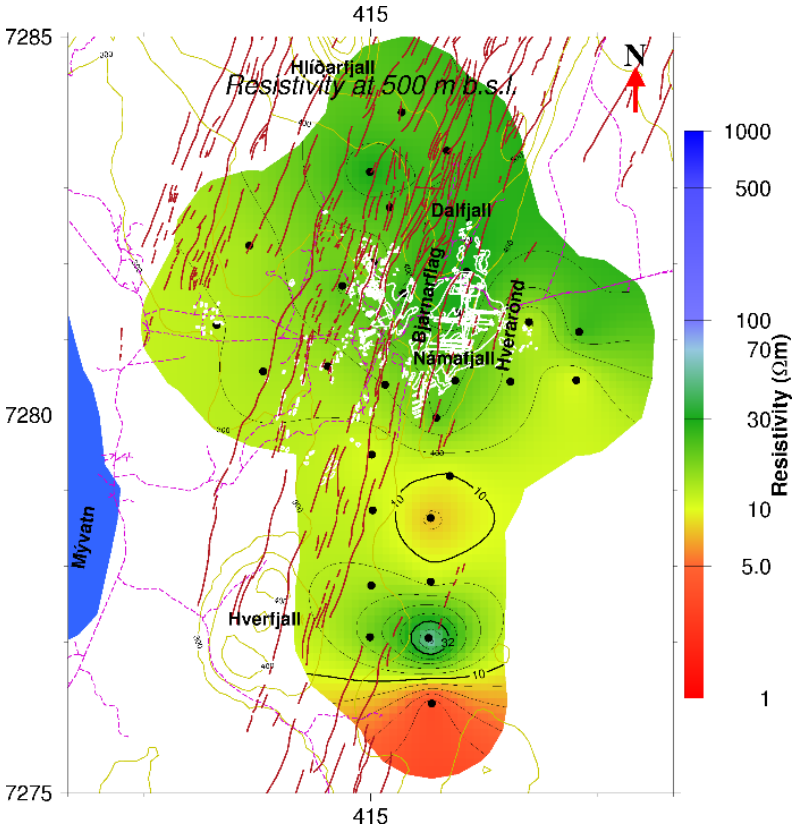

FIGURE 43: Námafjall, iso-resistivity map at 500 m b.s.l.; symbols are explained in the caption of Figure 41

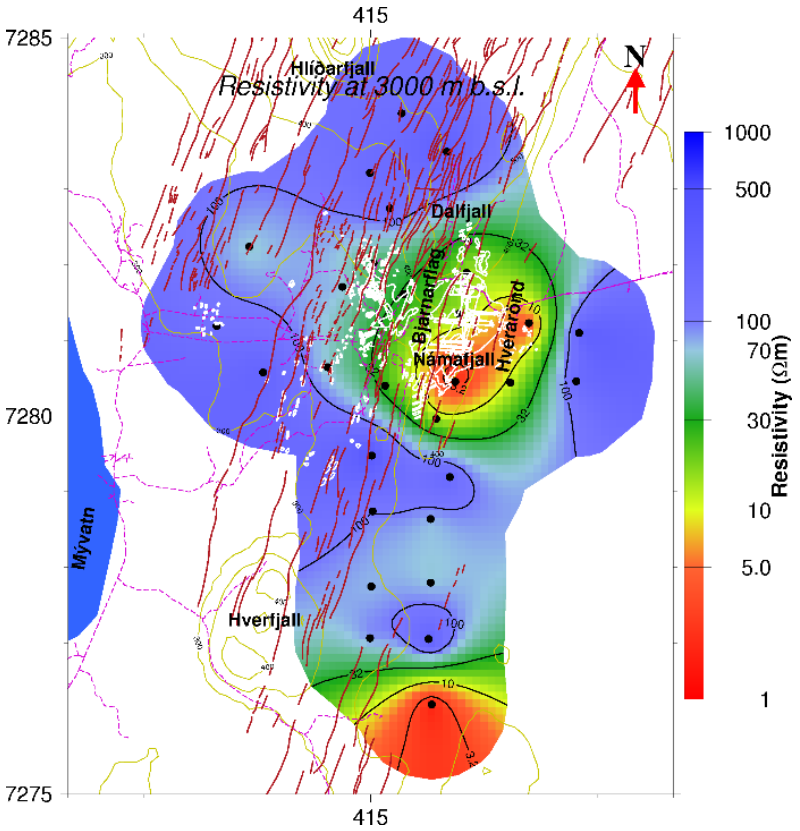

FIGURE 44: Námafjall, iso-resistivity map at 3000 m b.s.l.; symbols are explained in the caption of Figure 41

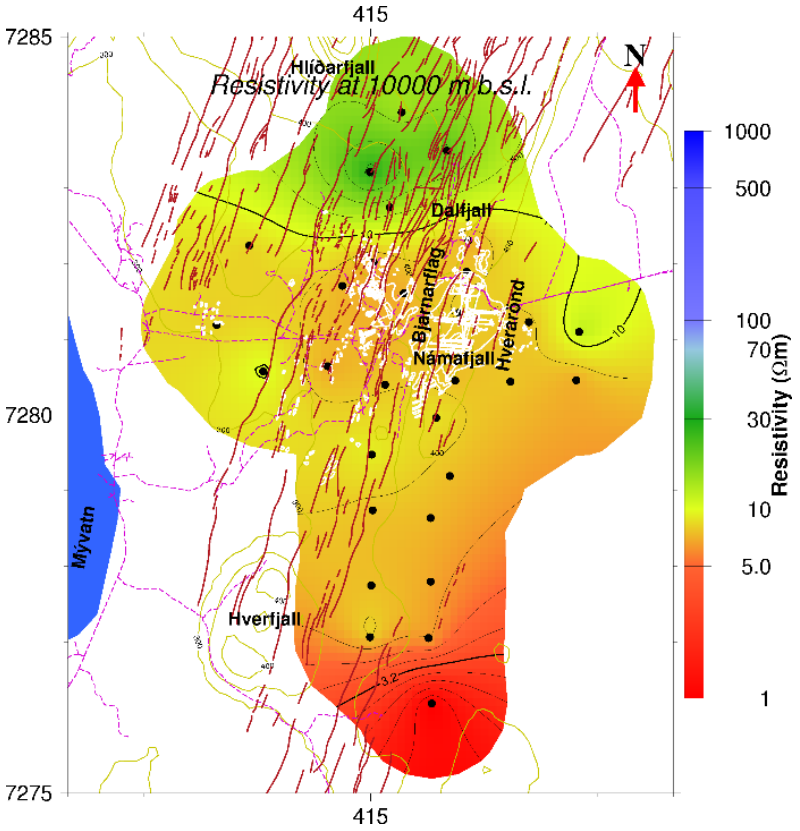

FIGURE 45: Námafjall, iso-resistivity map at 10,000 m b.s.l.; symbols are explained in the caption of Figure 41

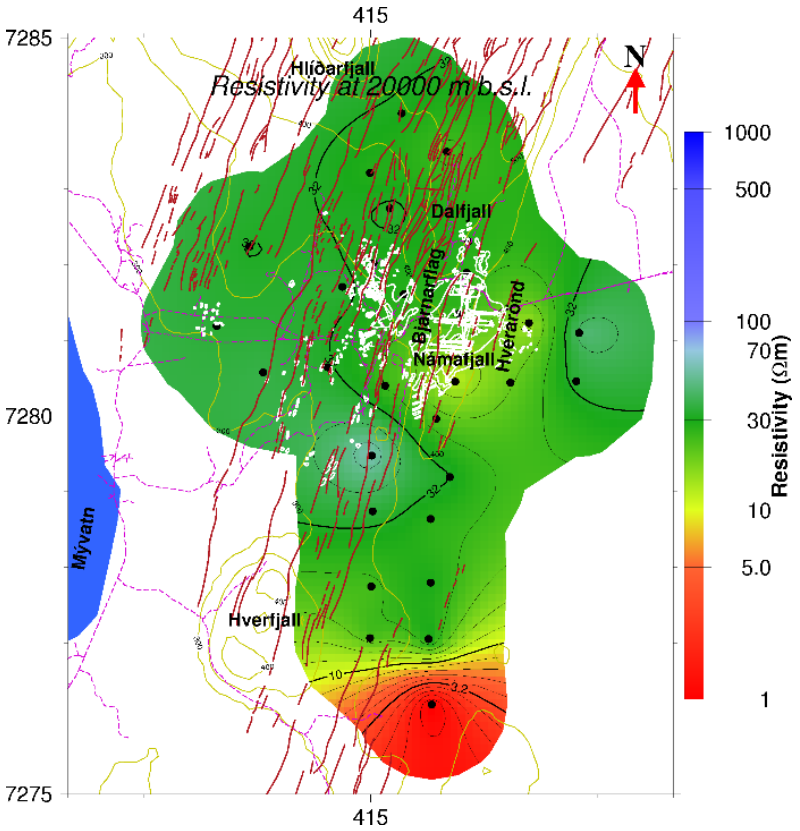

FIGURE 46: Námafjall, iso-resistivity map at 20,000 m b.s.l.; symbols are explained in the caption of Figure 41

9.7 Comparison of 1D joint inversion of TEM and MT with boreholes

Borehole BJ-14 is near MT sounding 010 (Figure 28). This is a directional well and drilled from east to west. This borehole is located close to the W-E profile and was projected on to the cross-section. There is a good match between the resistivity and the temperature and alteration minerals in the top and bottom parts of the borehole. In the borehole's lithology, the chlorite minerals appear at less than 150°C and resistivity at that position is low, which is a mismatch. The major reason for this mismatch is that the well is not vertical and does not really lie on the profile, so the projection of the well on the cross-section does not represent the actual depth (Figure 47).

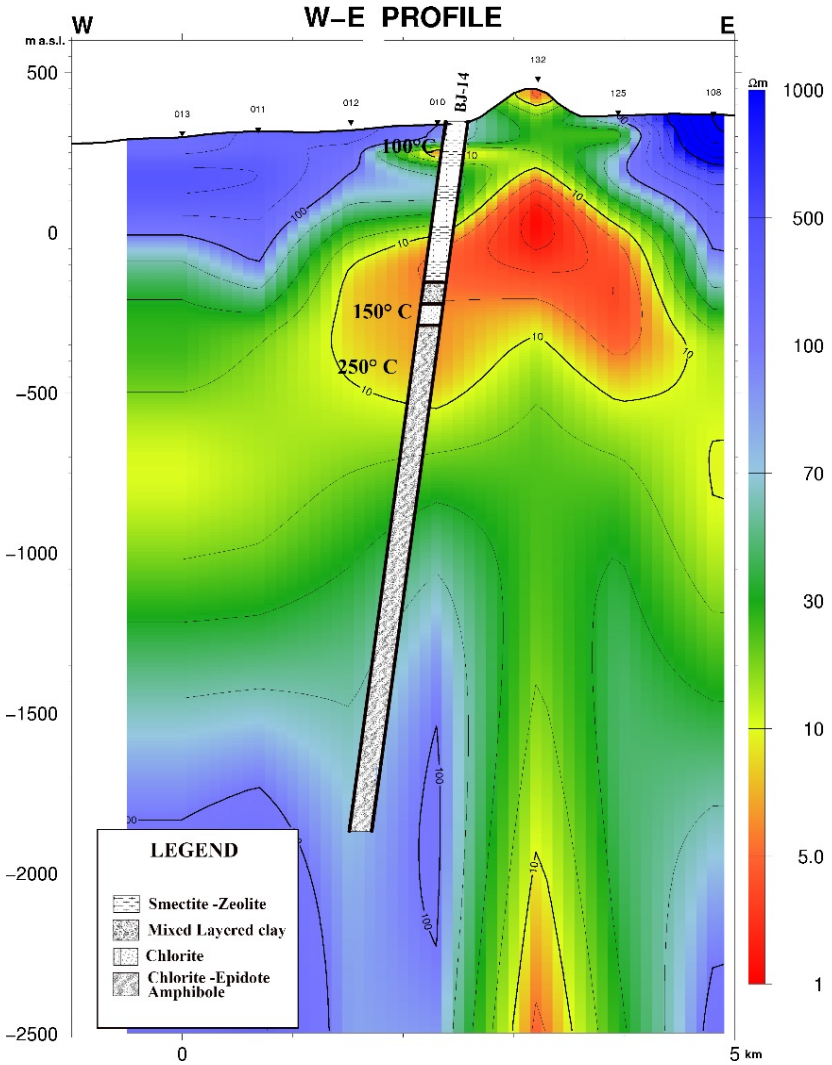

FIGURE 47: Námafjall, resistivity of the W-E profile correlated with borehole lithology

10. CONCLUSIONS AND RECOMMENDATIONS

- The depth of penetration of TEM is heavily dependent on resistivity. Most of the TEM data show a depth of penetration of 1000 m for a current of 2.5 Hz transmitted frequency.
- Static shift is a problem for MT and it can be removed by joint inversion of TEM and MT data.

- The study area has a shift factor of both less than one and higher than one. In Námafjall and north of Hverfjall area, MT data suffer upward shift and the area has a conductive anomaly near the surface. MT data in the unaltered surface area suffer downward shift; this area has a resistive anomaly.
- The MT data have a depth of penetration of about 30 km. Joint inversion indicates that there is a low-resistivity anomaly below Námafjall ridge and its extension below the surface coincides with the conceptual model of Krafla. This zone marks the low-resistivity cap that presents zeolites and smectite type clay, while the underlying high-resistivity core below it has epidote and chlorite minerals. The presence of a conductive body is also identified by the Tipper strike. Some fractures across the main fault direction are indicated by the Tipper strike near the Hverfjall area. There is a low-resistivity layer at a depth of 800 m in the northernmost side of the study area that probably indicates a connection between Krafla and this field.
- There is a low-resistivity zone below the Námafjall ridge, between 3 and 10 km which might represent the heat source for this high-temperature area.
- Finally, further detailed study with other available information is needed to characterise the area. Joint study of TEM and MT is very useful for deep-seated structures. This method for studying the subsurface will give positive results in Bangladesh, if the cultural noise is minimized during data collection.

ACKNOWLEDGEMENTS

I would like to thank the Government of Iceland for bearing all the expenses of the United Nations University Geothermal Training Programme (UNU-GTP) and awarding me a fellowship through UNU-GTP in order to attend this course. I would like to express my deepest gratitude to Dr. Ingvar B. Fridleifsson, Director, and Mr. Lúdvík S. Georgsson, Deputy Director, of the United Nations University, Iceland, for giving me the opportunity to take part in this training programme in 2012.

I am sincerely grateful to my supervisors, Mr. Gylfi Páll Hersir and Mr. Andemariam Teklesenbet Beyene for their assistance and daily advice during the study time. I wish to thank Mr. Ingimar Gudni Haraldsson, Mr. Markús A.G. Wilde and Ms. Málfrídur Ómarsdóttir for their continuous guidance, moral support and enthusiastic help for the preparation of my report and during the training programme.

Finally, I am grateful to DG of Geological Survey of Bangladesh, Energy and Mineral Resources, Government of the People's Republic of Bangladesh, for allowing me to attend the course.

REFERENCES

Árnason, K., 2006a: *TemX. A graphically interactive program for processing central-loop TEM data, short manual.* ÍSOR – Iceland GeoSurvey, Reykjavík, 10 pp.

Árnason, K., 2006b: *TEMTD (Program for 1D inversion of central-loop TEM and MT data)*. ÍSOR – Iceland GeoSurvey, Reykjavík, short manual, 16 pp.

Árnason, K., 2008: *The magneto-telluric static shift problem*. ÍSOR – Iceland GeoSurvey, Reykjavík, report ISOR-08088, 17 pp.

Árnason, K., Karlsdóttir, R., Eysteinsson, H., Flóvenz, Ó.G., and Gudlaugsson, S.Th., 2000: The resistivity structure of high-temperature geothermal systems in Iceland. *Proceedings of the World Geothermal Congress 2000*, *Kyushu-Tohoku, Japan,* 923-928.

Cagniard, L., 1953: Basic theory of the magneto-telluric method of geophysical prospecting. *Geophysics, 18,* 605-635.

Dakhnov, V.N., 1962: Geophysical well logging. *Q. Colorado Sch. Mines, 57-2*, 445 pp.

Flóvenz, Ó.G., Hersir, G.P., Saemundsson, K., Ármannsson, H., and Fridriksson, T., 2012: Geothermal energy exploration techniques. In: Sayigh, A. (ed.), *Comprehensive renewable energy*, *Vol. 7.* Elsevier, Oxford, 51-95.

Freie Universität Berlin, 2008: *Magnetotellurics*. Freie Universität Berlin, webpage: userpage.fu-berlin.de/~mtag/MT-principles.html.

Google Earth, 2012: *Maps.* Google Earth, webpage: *maps.google.com*

Guha, D.K., and Henkel, H., 2005: Abandoned on-shore deep wells – a potential geothermal energy resource for rural Bangladesh. *Proceedings of the World Geothermal Congress 2005, Antalya, Turkey,* 11 pp.

Guha, D.K., Henkel, H., and Imam B., 2010: Geothermal potential in Bangladesh - results from investigations of abandoned deep wells. *Proceedings of the World Geothermal Congress 2010, Bali, Indonesia,* 8 pp.

Gudmundsson, Á., Mortensen, A.K., Hjartarson, A., Karlsdóttir, R., and Ármannsson, H., 2010: Exploration and utilization of the Námafjall high-temperature area in N-Iceland. *Proceedings of the World Geothermal Congress 2010, Bali, Indonesia,* 9 pp.

Heath, R.C., 2004: *Basic ground-water hydrology* (10th printing). USGS, Reston, Virginia, 86 pp.

Hersir, G.P., 2012*: Resistivity of rocks.* UNU-GTP, Iceland, unpublished lecture notes.

Hersir, G.P., and Árnason, K., 2009: Resistivity of rocks. *Paper presented at the "Short Course on Surface Exploration for Geothermal Resources", organized by UNU-GTP and LaGeo, Santa Tecla, El Salvador,* 8 pp.

Hersir, G.P., and Björnsson, A., 1991: *Geophysical exploration for geothermal resources. Principles and applications*. UNU-GTP, Iceland, report 15, 94 pp.

Hersir, G.P., Árnason, K., and Vilhjámsson A.M., 2012: *3D inversion of MT data from Krýsuvík, SW Iceland.* Draft article to be presented at the Geothermal Workshop in Stanford, 2013.

Jones, A., 1988: Static shift of MT data and its removal in a sedimentary basin environment. *Geophysics, 53,* 967-978.

Kearey, P., Brooks, M., and Hill, I., 2002: *An introduction to geophysical exploration* (3rd ed.). Blackwell Scientific Publications, Oxford, 262 pp.

Malimo S.J., 2012: *Aquifer fluid modelling and assessment of mineral-gas-liquid equilibria in the Námafjall geothermal system, NE-Iceland*. University of Iceland, MSc thesis, UNU-GTP, report 3, 67 pp.

Mortensen, A.K., Jónsson, S.S., Richter, B., Danielsen, P.E., Sigurdsson, Ó., Birgisson, K., Mahmood, A.T.K., and Gíslason, J., 2006: *Trölladyngja – borehole TR-02, 3. phase: Drilling for 9⅝"slotted liner from 800 m to 2280 m depth.* Iceland GeoSurvey, Reykjavík, report 2006/060 (in Icelandic), 75 s.

Nicholson, H., Condomines, M., Fitton, J.G., Fallick, F.E., Grönvold, K., and Rogers, G., 1991: Geochemical and isotopic evidence for crustal assimilation beneath Krafla, Iceland. *J. Petrol., 32,* 1005-1020.

Pálmason, G., and Saemundsson, K., 1974: Iceland in relation to the Mid-Atlantic Ridge. *Ann. Rev. Earth Planet. Sci., 2,* 25-63.

Pytte, A.M., and Reynolds, R.C., 1989: The thermal transformation of smectite to illite. In: Naeser, N.D., and McCulloh, T.H. (eds.), *Thermal history of sedimentary basins*. Springer-Verlag, NY, 51-64.

Quist, A.S., and Marshall, W.L., 1968: Electrical conductances of aqueous sodium chloride solutions from 0 to 800°C and at pressures to 4000 bars. *J. Phys. Chem., 72*, 684-703.

Rahman, M., 2006: Geothermal potential resources in Thakurgaon district, northern Bangladesh. *Bangladesh J. Geology, 25,* 13-30.

Rowland, B.F., 2002: *Time-domain electromagnetic exploration.* Northwest Geophysical Associates, Inc., 6 pp.

Saemundsson, K., 2010: *Námafjall. Geological and geothermal map, 1:25000.* Landsvirkjun and ÍSOR – Iceland GeoSurvey.

Sakindi, G., 2012: Analysing the subsurface resistivity structure on two profiles across the Námafjall high-temperature geothermal field, NE-Iceland, through 1D joint inversion of TEM and MT data**.** Report 30 in: *Geothermal training in Iceland 2012.* UNU-GTP, Iceland, 733-768.

Scales, J.A., Smith, M.L., and Treitel, S., 2001: *Introductory geophysical inverse theory.* Samizdat Press, Colorado School of Mines, 189 pp.

Stephen, J., Gokarn, S.G., Manoj, C., and Singh, S.B., 2003: Effects of galvanic distortions on magnetotelluric data: Interpretation and its correction using deep electrical data. *J. Earth System Science, 112-1,* 27-36.

Sternberg, K.B., Wasburne, J.C., and Pellerin, L., 1988: Correction for the static shift in magnetotellurics using transient electromagnetic soundings. *Geophysics, 53-11,* 1459-1468.

Tikhonov, A.N., 1950: The determination of electrical properties of the deep layers of the earth's crust. *Dokl. Acad. Nauk., SSR 73,*295-297 (in Russian).

Tucker, M.E., 1991: *Sedimentary petrology* (2nd ed.). Blackwell Scientific Publ., London, 260 pp.

Uddin, M.Z., 2012: *Appendices to the report "1D joint inversion of TEM and MT resistivity data with an application of soundings from the Námafjall high-temperature geothermal area, NE-Iceland"*. UNU-GTP, Iceland, report 35 appendices, 30 pp.

Unsworth, M., 2012: *Theory of magnetotellurics over a 1-D Earth.* University of Alberta, Edmonton, Canada, webpage: *www.ualberta.ca/~unsworth/UA-classes/424/notes424/424D1-2012.pdf.*

USDOT, 2012: *Mapping lithology*. US Department of Transportation, webpage: *www.cflhd.gov/resources/agm/engApplications/SubsurfaceChartacter/613MappingLithology%281%29.cfm.*

Wightman, W.E., Jalinoos, F., Sirles, P., and Hanna, K., 2003: *Application of geophysical methods to highway related problems*. Federal Highway Administration, Central Federal Lands Highway Division, Lakewood, CO, Publication No. FHWA-IF-04-021.

Wikipedia, 2012: *Bangladesh Thakurgaon District*. Wikipedia, webpage: *en.wikipedia.org/wiki/File:Bangladesh_Thakurgaon_District.png.*